



# Rainfall-induced landslide prediction models, part ii: deterministic physical and phenomenologically models

Kyriillos M. P. Ebrahim<sup>1,2</sup> · Sherif M. M. H. Gomaa<sup>1,2</sup> · Tarek Zayed<sup>1</sup> · Ghasan Alfalah<sup>3</sup>

Received: 20 October 2023 / Accepted: 25 January 2024  
© The Author(s) 2024

## Abstract

Landslides are frequent hillslope events that may present significant risks to humans and infrastructure. Researchers have made ongoing efforts to assess the potential danger associated with landslides, intending to ascertain the location, frequency, and magnitude of these events in a given area. This study is meant to supplement the previous study (Part I), which explored empirical and physically based causative thresholds. In this paper (Part II), a systematic review is used to conduct an in-depth study of existing research on prediction models. Deterministic physical approaches were investigated for local-scale landslides. Next, national-scale landslide susceptibility models are discussed, including qualitative and quantitative models. Consequently, key findings about rainfall-induced landslides are reviewed. The strategy selection is generally governed by data and input factors from a macroscopic perspective, while the better prediction model is defined by dataset quality and analysis model performance from a microscopic perspective. Physically based causative thresholds can be used with limited geotechnical or hydrological data; otherwise, numerical analysis provides optimal accuracy. Among all statistical models, the hybrid artificial intelligence model achieved the best accuracy. Finally, current challenges have concentrated on integrating AI and physical models to obtain high accuracy with little data, prompting research suggestions. Advanced constitutive models for real-time situations are lacking. Dynamic and spatiotemporal susceptibility maps are also used, although their subjectivity needs further research. This study analyses how to choose the best model and determine its key traits. This research provides valuable insights for scholars and practitioners seeking innovative approaches to lessen the severity of landslides.

**Keywords** Landslides · Prediction · Rainfall · Deterministic physical models · Phenomenological models

## Introduction

Landslides are the downward displacement of hillslope soil. They are a prevalent hazard in sloping terrestrial areas, causing fatalities, infrastructure damage, and economic losses

(Chae et al. 2020), whereas rainfall-induced shallow landslides are extremely dangerous (Das et al. 2022; Formetta and Capparelli 2019; Saadatkhah et al. 2015; Thang et al. 2022; Ebrahim et al. 2024a, b). Regardless of the authorities' attempts to reduce the danger of landslides, such catastrophes require further study to accurately predict when and where landslides will occur. Figure 1 presents the number of humans killed by landslides from 1 August to 31 December 2020, according to the European Commission's Directorate-General for European Civil Protection and Humanitarian Aid Operations in 2022. Online: Global overview of landslides with fatalities (1 August – 31 December 2020)—World 1 ReliefWeb (Visited on July 10, 2023).

Landslides can be classified into four sizes based on their volume: smaller (less than 200 m<sup>2</sup>), small (between 200 and 2000 m<sup>2</sup>), medium (between 2000 and 10,000 m<sup>2</sup>), and huge (more than 10,000 m<sup>2</sup>) (Medwedeff et al.

✉ Sherif M. M. H. Gomaa  
sherif.gomaa@polyu.edu.hk

<sup>1</sup> Department of Building and Real Estate, Faculty of Construction and Environment, The Hong Kong Polytechnic University, Hung Hom, Kowloon, Hong Kong  
<sup>2</sup> Structural Engineering Department, Faculty of Engineering, Mansoura University, Mansoura, Egypt  
<sup>3</sup> Department of Architecture and Building Sciences, King Saud University, Riyadh, Saudi Arabia

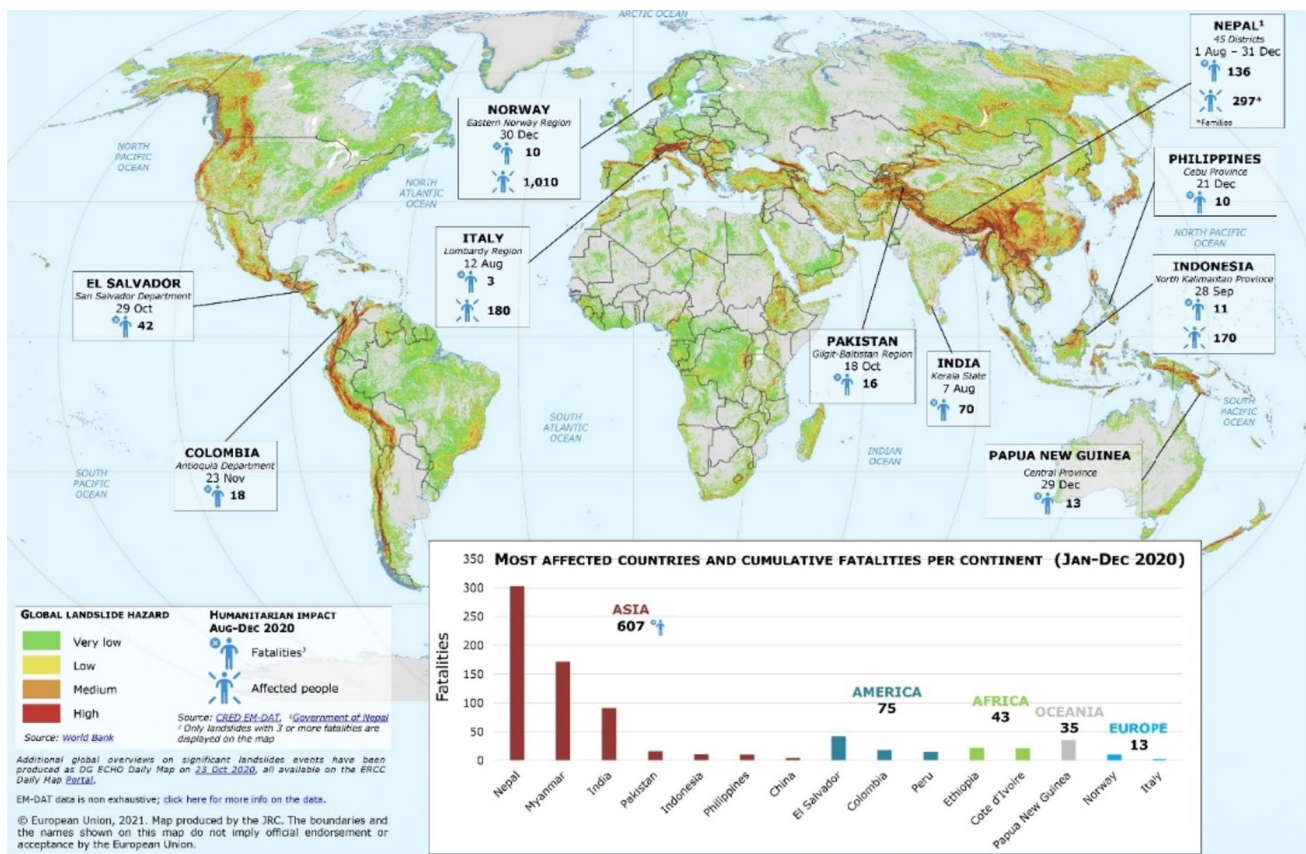


**Fig. 1** World map showing the number of people killed by landslides between 1 August and 31 December 2020: Figure adapted with permission from European Civil Protection and Humanitarian Aid Operations; Copyright European Union, 2021

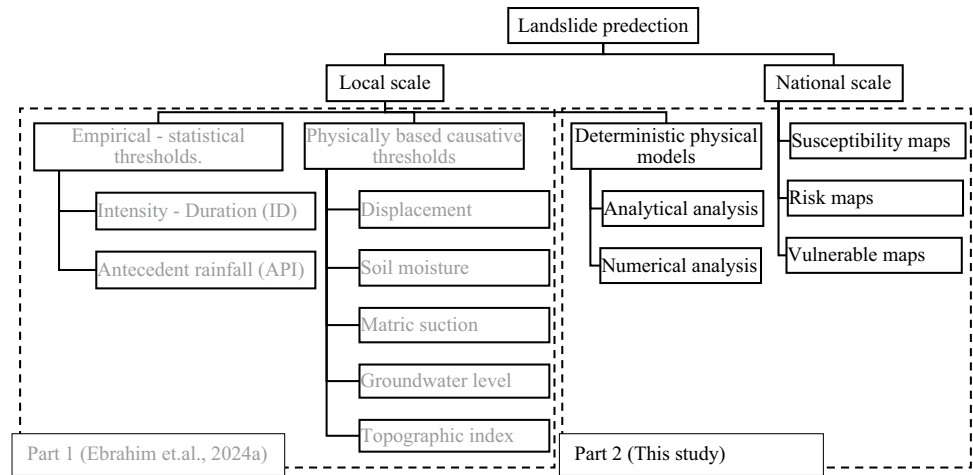
2020). Furthermore, landslides can be studied from two perspectives: local (i.e., single slope to 10 km<sup>2</sup>) and national scales (i.e., hundreds to thousands of km<sup>2</sup>) (Oguz et al. 2022). Thus, prediction models have been classified according to the scale of the landslide. Empirical and physical models are suitable for local scales (Bednarczyk 2018; Cao et al. 2020; Davar et al. 2022; Ho et al. 2012; Hong et al. 2018; Wu et al. 2015; Zhao et al. 2019); however, susceptibility, risk, and vulnerability maps are acceptable for national scales (Anbalagan et al. 2015; Bezerra et al. 2020; Ng et al. 2021; Shah et al. 2023). It should be emphasized that the danger of inaccurate or missing projections should be considered while evaluating landslide prediction models, considering the projected cost of infrastructure damage and the size of the afflicted population zone (Zhao et al. 2019). Figure 2 depicts the prediction models' categorization, illuminating the local and national scale models.

Earthquakes, volcanoes, floods, and intense rainstorms may all cause landslides (Román-Herrera et al. 2023). Massive landslides, which are becoming more prevalent as a

result of climate change, can be triggered by rainstorms (Wu et al. 2020; Zhao et al. 2019). As a result, this study focuses on prediction methodologies for rainfall-induced landslides, the majority of which are shallow landslides (Das et al. 2022; Saadatkhah et al. 2015; Thang et al. 2022). Shallow landslides have a slip surface parallel to the ground surface and a depth of 2 to 5 m (Caine 1980; Huang et al. 2015; Zhang et al. 2011; Liu et al. 2022). Because of their quick development and severity, shallow landslides are more dangerous than deep-seated ones (Formetta and Capparelli 2019).

Slope stabilization, monitoring, and prediction are viable approaches to decrease landslide risk. Stabilizing piles, soil nailing, drainage channels, and other mitigation techniques are required whenever the slope system is subjected to an unexpected event (such as rainfall or an earthquake) or degradation of geotechnical components (Huang and He 2023): however, stabilizing the entire slope is not a practical solution. Landslide monitoring and prediction must be carried out to prioritize stabilizing the crucial slope. Landslide monitoring tracks and gathers data to understand better and study the phenomena (De Graff 2011). However, choosing the most

**Fig. 2** Classifications of landslide prediction models



effective monitoring system necessitates a detailed understanding of the factors that cause occurrences (initial conditions). For example, tilt measurement may not be appropriate for transitional landslides caused by limited toe support or for slow slope changes since tilting is uncommon under such conditions (Giri et al. 2018; Ma et al. 2017). Ebrahim et al. (2024b) discuss the most recent developments in landslide monitoring, which is different from the topic of this work.

According to Liang and Uchida (2022), using landslide prediction models can aid in mitigating the extent of damage caused by landslides triggered by rainfall and develop disaster alert systems. It is crucial to employ landslide prediction models for some reasons. They can first assist in identifying areas that are susceptible to landslides. The danger can be decreased with the information given, for instance, by building retaining walls or adding vegetation. Second, landslide prediction models can provide an early warning of potential landslides. According to Valentino et al. (2014), this gives authorities the ability to protect houses and rescue people, perhaps averting casualties and property damage. Thus, this study aims to investigate the main factors that affect landslides triggered by rainfall, focusing on the critical role that each factor plays in obtaining precise predictions of landslide events.

This study will employ quantitative (scientometric) and qualitative (systematic) methodologies to address the existing research. Referring to Fig. 2, many landslide prediction techniques (empirical-statistical thresholds, physically based causative thresholds, physical analytical and numerical models, and landslide susceptibility analysis) will be illustrated in two articles. The first is restricted to physically based causative thresholds and empirical-statistical thresholds (Ebrahim et al. 2024a). In the second (this research), deterministic models and models for landslide susceptibility analysis are included. Several statistical approaches (e.g., statistical regression, artificial intelligence, probabilistic, and mathematical analytical models) are combined with landslide prediction. Table 1

summarizes several review papers that discuss landslide prediction techniques based on the authors' knowledge and data that is available. A large number of them focus on a specific methodology and approach. Utilizing scientometric analysis has been rare. Thus, the following is how the innovation of this work might be expressed:

1. A bibliometric analysis is used in conjunction with a combined scientometric and systematic review to assess the accuracy of various models.
2. The theoretical geotechnical and hydrological concept of rainfall-induced landslides is provided with an extensive illustration of the initial condition.
3. This study's Parts I and II include nearly all current prediction techniques, including deterministic physical models, physically causative models, empirical statistical thresholds, and landslide susceptibility maps.
4. This analysis focuses on current research being used till 2023.

This study is organized as follows: The systematic study is described in Section "Systematic review", which is separated into two subsections: a) deterministic physical models and b) landslide susceptibility. "Research gaps and future directions" highlights the research gaps and future directions; Section "Conclusions" provides the conclusion; "Acknowledgements" acknowledges contributions; "Notations and Abbreviations" describes the notations and abbreviations; and "References" lists the sources.

## Systematic review

### Deterministic physical models

Empirical and physically based causative thresholds can be applied easily for early warning systems. Complex

**Table 1** Related review articles for landslide prediction techniques are available

Study	Year	Approach	Content
(Zhang et al. 2011)	2011	Systematic	The concept of rainfall-induced landslides is considered from geotechnical and hydrological perspective
(Soga et al. 2016)	2016	Systematic	Modeling of unsaturated soil using the material point method
(Chae et al. 2017)	2017	Systematic	Landslide susceptibility, runout modeling, landslide monitoring, and early warning
(Segoni et al. 2018)	2018	Systematic	Rainfall thresholds
(Merghadi et al. 2020)	2020	Systematic	Algorithms for machine learning in landslide susceptibility
(Shano et al. 2020)	2020	Systematic	Several prediction techniques focus on statistical models
(Yanbin et al. 2022)	2022	Systematic	Machine learning models for assessing landslide susceptibility
(Zou and Zheng 2022)	2022	Scientometric	Scientometric analysis, limited physical prediction methods, and case studies
(Huang et al. 2022)	2022	Bibliometric	Landslide susceptibility based on GIS data
(Petrucci 2022)	2022	Systematic	The primary causes of landslide fatalities
(Yerro et al. 2022)	2022	Systematic	Modelling of unsaturated soil using the material point method
(Yusof et al. 2023)	2023	Systematic	Application of support vector machines in landslide susceptibility mapping
(Bhardwaj and Singh 2023)	2023	Systematic	Landslide susceptibility based on GIS data

physically based models provide accurate results compared with these models, excluding the cost and modelling complexity of these models. A comparison between physically based models and empirical thresholds indicates that physically based models provide accurate predictions (Ho and Lee 2017; Wang et al. 2020; Zhao et al. 2019). Deterministic physical analysis combines both the hydrological process and slope stability analysis.

Landslides occur as a result of changes in pore water pressures and seepage forces throughout the hydrological process (Gerscovich et al. 2006). Generally, it is assumed that saturated steady-state flow occurs over a given depth. Thus, the safety factor is calculated considering the worst case (Collins and Znidarcic 2004; Ho et al. 2012). In this case, there is no effect of rainfall, while under rainfall conditions, infiltration is one of the leading causes of initially unsaturated landslides (Formetta and Capparelli 2019). In saturated–unsaturated soil systems, the partial differential equations that may be used to calculate infiltration and soil moisture profiles using Darcy's law and unsaturated flow equations are rather complicated (refer to Eq. 1) (Richards 1931). Therefore, many analytical models, such as the widely used model developed by Green and Ampt (1911), consider some assumptions of the initial conditions to simplify the infiltration process. Some of these analytical models include the GR4J model (Perrin et al. 2003), TOPMODEL (Kirkby and Beven, 1979), SHETRAN (Birkinshaw and Ewen 2000), SIMTOP (Lee and Ho 2009), Modified Green–Ampt (Cho 2017), Modified TOPMODEL (Lee and Ho 2009), CREST (Wang et al. 2011), TiVaSS (An et al. 2016), TRIGRS (Baum et al. 2008), HIRESSS (Rossi et al. 2013), H-SLIDER (Uchida et al. 2009), TAG-FLOW (Thang et al. 2022), and SLIP (Valentino et al. 2014). Nevertheless, this approach fails to take into account the influence of the

slope and variations in rainfall intensity. Thus, in order to get more precise data, it is essential to find the solution to the complicated equation. The numerical analysis integrates more advanced models of hydraulic properties (Rahimi et al. 2010). Prime examples of such applied models in landslide analysis include GeoStudio (Geo-slope) (Das et al. 2022; Huang and He 2023; Xu et al. 2022; Calvello et al. 2009; Pagano et al. 2010; Wan et al. 2017); MIDAS/GTS (Qiu et al. 2019; Yang et al. 2023); ABAQUS (He et al. 2021); GEOTop 2.0 (Formetta and Capparelli 2019); Rocscience software (RS2) (Purnama et al. 2022); BGSlope (Abolmasov et al. 2015); SLIDE (He et al. 2016; Khan and Wang 2021; Liao et al. 2010); and PLAXIS (Arinze et al. 2021; Oguz et al. 2022).

$$\frac{\partial}{\partial x} \left( k \frac{\partial h_w}{\partial x} \right) + \frac{\partial}{\partial y} \left( k \frac{\partial h_w}{\partial y} \right) + \frac{\partial}{\partial z} \left( k \frac{\partial h_w}{\partial z} \right) = -\frac{\partial \theta_w}{\partial t} \quad (1)$$

where  $\theta_w$  is the volumetric water content,  $k$  is the unsaturated hydraulic conductivity, and  $h_w$  is the total head.

In the case of rainfall, the wetting front concept can be used to simplify matric suction. The following is how the suction effect is recognized: The suction rises during the dry season as a result of evapotranspiration and falls during the rainy season as a result of infiltration (Pagano et al. 2010). The difference between the air pressure and the pore water pressure in the unsaturated soil is the matric suction, which attracts water (He et al. 2021). The pore water pressure distribution can be classified into steady-state conditions and transient states, as shown in Fig. 3. The transient state is a transitional state between the initial state and the final state. Thus, the time required to reach the final state is a function of the hydraulic conductivity of the soil, ground surface flux, and water storage of the soil. The matric suction vanishes

when the surface flux ( $q$ ) exceeds or equals the saturated hydraulic conductivity ( $k_{sat}$ ). Otherwise, the matric suction decreases. It should be noted that the variation in pore water pressure due to rainfall will affect the stresses and deformation of the soil. This makes the infiltration and seepage analysis more complex; thus, numerical analysis is required (Zhang et al. 2011). Soil hydraulics and shear strength parameters are essential for better prediction of saturated and unsaturated medium, which can be illustrated through the soil water characteristic curve (SWCC) and hydraulic conductivity function (HCF) (Das et al. 2022; Xu et al. 2022). The SWCC can be accurately defined by Mualem-van Genuchten (MVG) and Van Genuchten's model (Schaap and van Genuchten 2006).

Concerning the geotechnical model, the hydrological model can be combined with slope stability analysis to consider both the infiltration process and failure criteria, such as

Mohr-column failure criteria for unsaturated soil, as shown in Eq. 2 (Fredlund and Rahardjo 1993). It is reasonable to assume infinite slope stability because the depth of the failure surface to its length is shallow. Additionally, if the slope angle does not vary significantly along the slope height, the failure surface can be assumed to be parallel to the slope surface (Cho 2017; Ho and Lee 2017; Ho et al. 2012; Lee and Ho 2009; Wang et al. 2020; Wu et al. 2015). Furthermore, failure is assumed to be created between the surface soil and the bedrock layer. However, the failure surface can be above or at the soil–bedrock interface (Cho 2017; Thang et al. 2022; Valentino et al. 2014).

$$\tau = c' + (\sigma - u_a) \tan \phi' + \psi \tan \phi^b \tag{2}$$

where  $c'$  is the effective cohesion;  $\phi'$  is the effective friction angle;  $\psi = u_a - u_w$  is the matric suction;  $u_a$  is atmospheric

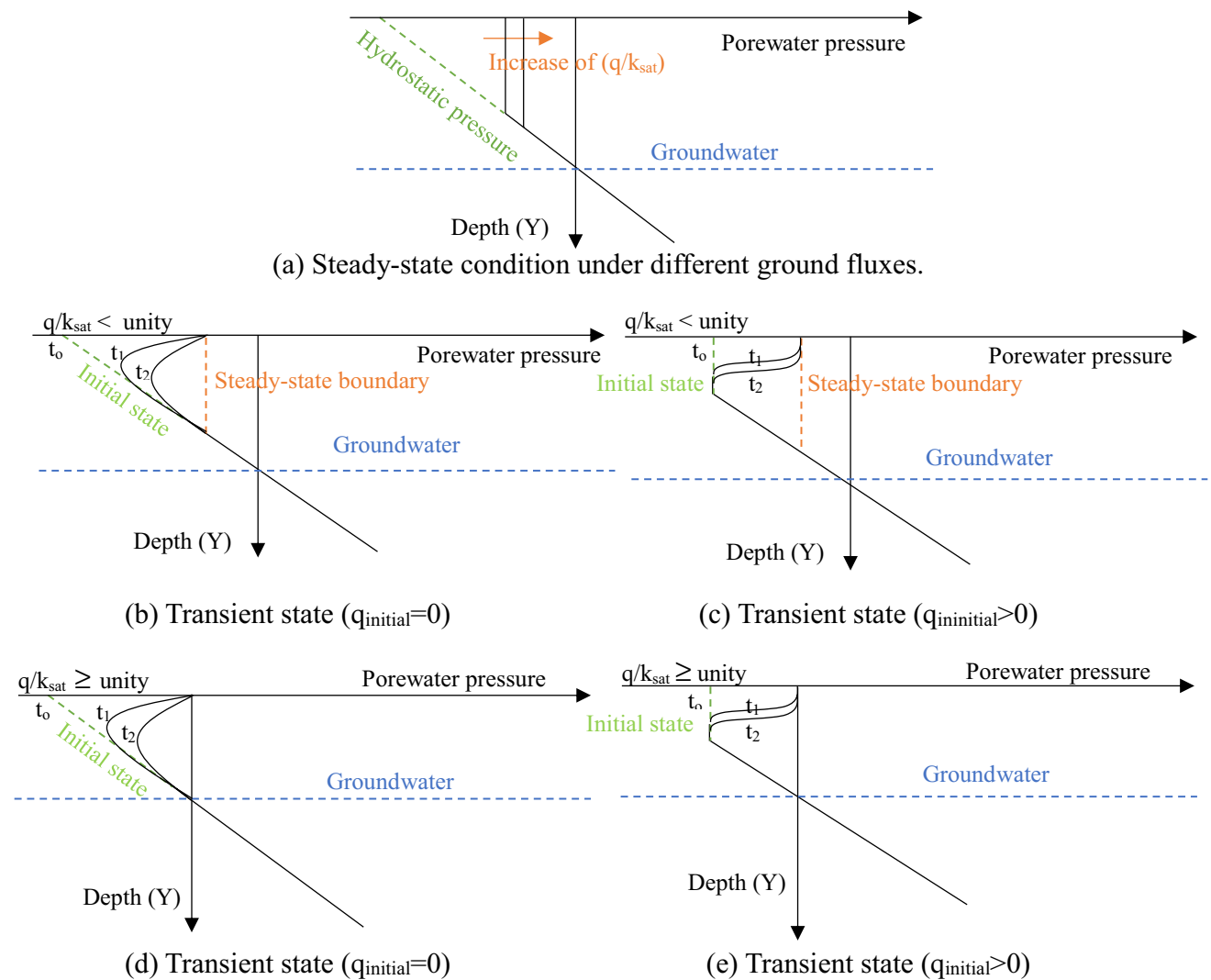


Fig. 3 Typical pore water pressure profile

pressure;  $u_w$  denotes the pore water pressure;  $\phi^b$  is the internal friction angle corresponding to the matrix suction; and  $\sigma$  is the total stress.

### Analytical models

Richards (1931) presents a 3D equation that suffers algorithmic and computational challenges when considering the subsurface response due to rainwater infiltration. Even so, it can be reduced using analytical models based on comprehending the true initial state of the case study (Huo et al. 2023). Analytical approaches can consider external factors such as rainfall and internal factors such as topographic, geological, geotechnical, and hydrological factors. By integrating susceptibility maps with analytical models, precise landslide occurrence predictions may be made. Models like this have a notable advantage regarding computational time and cost. As a result, to benefit from such analytical models, an in-depth understanding of the initial conditions is fundamental. Several assumptions and cases are emphasized in the following lines (Table 2 and 3).

To simplify, the suction effect might be disregarded in certain areas that experience persistent and intense rainfall, leading to saturation of the region. Based on these assumptions, the factor of safety and critical rainfall can be calculated as illustrated in Eqs. 3 and 4 (Ho et al. 2012). Nevertheless, as previously stated, the fluctuation in pore water pressure caused by rainfall will impact the stresses and deformation. Consequently, the

infiltration process is crucial and can be classified into steady-state and transient-state conditions. This classification is based on the approximations of the Richards equation. Logically, the transient state provides reliable and accurate data compared with steady-state models. This finding is based on the comparison between dynamic and steady-state models developed by Liang and Uchida (2022) and Valentino et al. (2014).

$$FS = \frac{C' + (H\gamma_t - h_w\gamma_w)g\cos^2\beta\tan\phi}{\gamma_t g H \sin\beta \cos\beta} \quad (3)$$

$$i_{cr} = T \sin\beta \left(\frac{a}{b}\right) \left[ \frac{C'}{\gamma_w g H \cos^2\beta \tan\phi} + \frac{\lambda_t}{\gamma_w} \left(1 - \frac{\tan\beta}{\tan\phi}\right) \right] \quad (4)$$

where  $FS$  is the factor of safety;  $C'$  is the effective cohesion;  $g$  is the gravitational acceleration;  $\gamma_t$  is the soil bulk density;  $\gamma_w$  is the water density;  $h_w$  is the saturated soil thickness above the slip surface;  $H$  is the soil thickness measured vertically;  $\beta$  is the gradient of the hill slope;  $\phi$  is the soil effective friction angle;  $i_{cr}$  the critical steady-state rainfall; and  $T$  is the saturated soil transmissivity.  $T = k_{sat} H \cos\beta$ , where  $k_{sat}$  is the saturated conductivity.

The 1D infiltration model is suitable for a thick or thin layer with free drainage from the bottom (Pagano et al. 2010). A widely used method called the Green Ampt (GA) (Green and Ampt 1911) method can provide a simple solution for the subsurface flow response. Based on Darcy's law, the GA assumes a 1D vertical infiltration through a uniform soil medium. Additionally, GA assumes the presence of a thin sheet of water at the ground surface. GA considers a consistent approach of the wetting front that divides the saturated wetting zone from the unsaturated soil zone with a constant value of soil matric suction (refer to Fig. 4). Using the Green-Ampt method, the infiltration rate can be measured as provided in Eq. 5.

**Table 2** Error matrix arrangement

The total population P + N		Predicted condition	
		Positive (PP)	Negative (PN)
Actual condition	Positive (P)	True positive (TP)	False negative (FN)
	Negative (N)	False positive (FP)	True negative (TN)

**Table 3** Landslide susceptibility ranges

Author	Landslide susceptibility ranges				
	Very low	Low	Moderate	High	Very high
(Zangmene et al. 2023)	3%		10%	21%	66%
(Sharma and Mahajan 2018)	0–2%	3%–9%	10%–16%	17%–23%	24%–89%
(Liao and Dennis 2004; Yang et al. 2012; Ng et al. 2021)	0–20%	20%–40%	40%–60%	60%–80%	80%–100%
(Dang et al. 2019)	0–19.2%	19.3%–41.8%	41.9%–58.2%	58.3%–77.2%	77.3%–100%
(Hua et al. 2021)	0–10%	10%–30%	30%–70%	70%–90%	90%–100%
(Yu et al. 2023)	0–50%	50%–75%	75%–85%	85%–95%	95%–100%
(Yang et al. 2022)	0.5%–9.8%	9.8%–26.8%	26.8%–43.5%	43.5%–64.6%	64.6%–96.9%
(Zhu and Huang 2006)	0–25%	25%–50%	50%–75%	75%–100%	

$$v = K_{sat} \frac{h \cos \beta + z_{\psi}}{h} \tag{5}$$

where:  $v$  is infiltration velocity;  $h$  is the depth of the moist peak shape perpendicular to the slope surface; and  $z_{\psi}$  is the matrix suction head at the moist peak shape.

A simple, theoretical, physically based approach assumes an infinite slope and combines Mohr–Coulomb and Darcy's laws, as shown in Eqs. 6 and 7 (Wu et al. 2015). The increase in pore water pressure causes the effective stress and strength to decrease. Therefore, it is assumed that the ratio between the height of the saturated layer and soil thickness determines the thresholds.

$$FS = \frac{\cot \beta \cdot [m_{sat}(n - 1) + G_s(1 - n) + n \cdot S_r(1 - m_{sat})] \tan \phi + \frac{2c'}{\sin 2\beta \cdot H \cdot \gamma_w}}{[m_{sat}(n - 1) + G_s(1 - n) + n \cdot S_r(1 - m_{sat})] + m_{sat}} \tag{6}$$

$$FS(t) = \frac{1}{N} \sum_{j=1}^N \left( \frac{C_j}{\rho_s g H_j \sin \beta_j \cos \beta_j} + \frac{\tan \phi_j}{\tan \beta_j} - \frac{\gamma_w \tan \phi_j}{\gamma_t H_j \tan \beta_j} \left[ H_j - \bar{Z}(t) - FRC \left( ATI - \ln \frac{W}{\tan \beta} \right)_j \right] \right) \tag{8}$$

where  $FS(t)$  represents the average  $FS$  of the sub-catchment at time  $t$ , and  $N$  indicates the number of grids in the sub-catchment. When  $FS(t) < 1$ , shallow landslides occur in the sub-catchment zone. Conversely, the hillslope is stable when  $FS(t) > 1$ .

Physically based models often focus on small catchments due to the significant computing load they impose (Wang et al. 2020). A coupled model, comprising the low-resolution hydrological model CREST (Coupled Routing and Excess STorage) developed by Wang et al. (2011) and the high-resolution slope stability model SLIDE (SLope-Infiltration-Distributed Equilibrium) proposed by He et al. (2016), is available for the prediction of landslides in a vast catchment area. The SLIDE model was used to forecast landslides; At the same time, this model assumes that the rainfall penetrates entirely into the soil. The CREST model simulates the hydrological process considering evaporation and runoff to overcome this drawback. The soil moisture using the TWI is then downscaled before it is used in SLIDE to link the hydrological model with the stability model (Wang et al. 2020). As mentioned above, the traditional Green-Ampt model assumes that water flows into a vertical homogeneous soil, which is infinite in depth. Therefore, Cho (2017) modified this equation to account for the initial inhomogeneous water content distribution and to simulate rainfall intensity smaller than the saturated hydraulic conductivity of the soil. When the rainfall intensity is lower than the saturated hydraulic conductivity of the overlying soil, the rain infiltrates to fill all the void space in the soil. Persistent rainfall leads to the upward displacement of soil caused by the refraction of the wetting front, resulting in

$$m_{sat(i,0)} = \frac{R_{i-1,i}}{n \cdot H \cdot (1 - S_r)} \cdot \exp \left[ -k \cdot \frac{\sin \beta}{n \cdot (1 - S_r)} (t_0 - t_i) \right], (i = 0, -1, -2, \dots) \tag{7}$$

where  $G_s$  is the specific gravity;  $n$  is the porosity;  $S_r$  is the degree of saturation;  $m_{sat}$  is the dimensionless thickness of the saturated layer which lies between 0 and 1;  $R_i$  is the rainfall depth;  $k$  is the infiltration rate; and  $t_0$  is the current time.

The infinite slope stability theory can involve stable and unstable grids based on the factor of safety calculated by Eq. 6. While previous researchers considered individual grid actions, shallow landslide prediction based on the Infinite Slope Model and TOPMODEL (SIMTOP) were used as hydrological models to assess the neighboring cell effect (Ho and Lee 2017). This can be illustrated as the stable neighboring cell assists the unstable cells until a sub-catchment reaches instability. Hence, the average factor of safety can be calculated from Eq. 8.

surface bonding. Upon reaching complete saturation, the soil ceases to allow any more infiltration, causing rainfall to runoff at the surface. Similarly, the groundwater variation and runoff analysis are taken into consideration using a modified version of TOPMODEL (TOPography-based hydrological MODEL). Groundwater is time-dependent and fluctuates with time (Lee and Ho 2009). Thus, assuming the failure surface is parallel to the slope surface, the factor of safety can be determined based on Eq. 9 (refer to Fig. 5).

$$FS = \frac{C' + (W_t \cos^2 \beta - \sigma_s) \tan \phi'}{W_t \sin \beta \cos \beta} \tag{9}$$

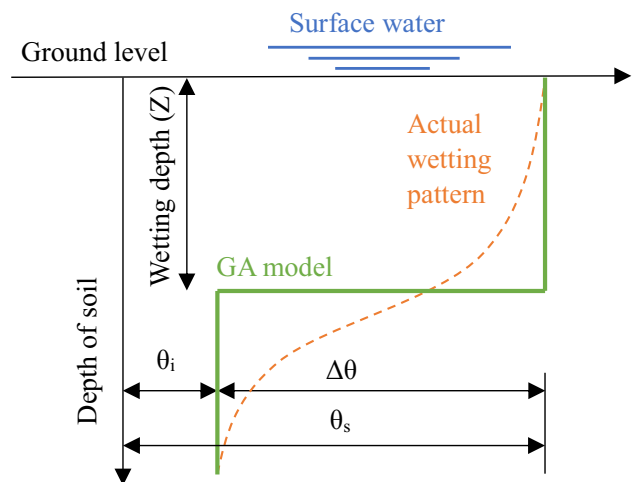


Fig. 4 GA real and assumed water content profile

where  $W_t$  is the weight of the soil slice, and  $\sigma_s$  is the suction stress expressed in terms of the normalized volumetric water content or effective degree of saturation  $S_r$ .

Furthermore, the TiVaSS model was created to address the significant non-linearity of the Richard equation in the 3D subsurface flow module. This was achieved by the use of partly implicit temporal discretization and the simplification of first-order spatial discretization (An et al. 2016). TiVaSS is coded in C++ and supports a GUI using the Qt framework. Assuming 1D infiltration, this model is vailed for uniform soil properties and initial pore water pressure without a horizontal flow. The results of both 3D Richard equations using numerical finite elements were comparable with results from TiVaSS, while TiVaSS has an advantage in computational cost (An et al. 2016). Similarly, TRIGRS is a transient rainfall infiltration and grid-based regional stability analysis model (Baum et al. 2008). The Richards equation's Iverson solution is used in the TRIGRS model. This model is coded using Fortran to consider the time-variant safety factor with rainfall conditions (refer to Eq. 10) assuming a rigid block in a sloping plane (Saadatkhah et al. 2015). PG-TRIGRS (probabilistic, geostatistic-based, transient rainfall infiltration, and grid-based slope stability) was developed to increase the accuracy by combining TRIGRS with probabilistic analysis (Salciarini et al. 2017).

$$FS = \frac{\tan\phi'}{\tan\beta} + \frac{c' - \psi(H, t)\gamma_w \tan\phi' *}{\gamma_t H \sin\beta \cos\beta} \tag{10}$$

where  $t$  is the time;  $\psi$  is the pore water pressure;  $C(\psi)$  is the specific moisture capacity;  $\theta$  is the volumetric water content;  $k_{sat}, k_{res}(\psi)$  is saturated and residual permeability;  $\phi'^* = \phi'$  if the magnitude of pwp is positive;  $\phi'^* = \phi^b$  if pwp is negative;  $\phi'$  is the soil friction angle;  $\phi^b$  is the friction angle related to the contribution of matric suction to the shear strength;  $\alpha$  is the parameter of SWCC.

Moreover, HIRESSS (HIgh-RESolution Slope Stability Simulator) was first developed by Rossi et al. (2013). In terms of hydrology, this model offers an analytical solution for Richard's equation that takes into consideration the dynamic response of infiltration. Geotechnically, this model considers the metric suction of unsaturated soil conditions and accounts for the vegetation index as a soil reinforcement (Salvatici et al. 2018). Vegetation has a positive impact on the cohesion parameter (Eq. 11), but has no effect on the friction angle. To accommodate this alteration, the factors of safety for unsaturated conditions and saturated conditions may be approximated using Eqs. 12 and 13, respectively.

$$C_{tot} = C' + fT_r(A_r/A) \tag{11}$$

$$FS = \frac{\tan\phi}{\tan\beta} + \frac{C_{tot}}{\gamma_d H \sin\beta} + \left( \gamma_w u_w \tan\phi \left\{ \left[ 1 + (h_b^{-1} |u_w|)^{\lambda+1} \right]^{\frac{\lambda}{\lambda+1}} \right\}^{-1} / \gamma_d H \sin\beta \right) \tag{12}$$

$$FS = \frac{\tan\phi}{\tan\beta} + \frac{C_{tot}}{(\gamma_d(H - u_w) + \gamma_{sat}u_w)\sin\beta} + \frac{\gamma_w u_w \tan\phi}{(\gamma_d(H - u_w) + \gamma_{sat}u_w)\tan\beta} \tag{13}$$

where  $T_r$  is the root failure strength,  $A_r/A$  is the root area ratio,  $f$  is a coefficient dependent on the effective soil friction angle and the orientation of roots,  $\gamma_d$  is the dry soil unit

weight,  $u_w$  is the pressure head,  $h_b$  is the bubbling pressure, and  $\lambda$  is the pore size index distribution.

For precise predictions, soil deterioration and weathering due to water level fluctuations must be considered. (Wan et al. 2017). A minimal internal friction angle should be expected since the water–rock contact went through several dry–wet cycles, resulting in zero cohesiveness. This process depends on hydrostatic pressure. To illustrate, Eqs. 14 and 15 present the degraded cohesion and internal friction angle when the hydrostatic pressure is 0.15 MPa. However, the abovementioned equations can give an illogical number of cycles; therefore, field interval tests are required to calibrate these equations.

$$c = c_0 [1 - 0.1149 \ln(1 + 0.2070 N^{1.8771})] \tag{14}$$

$$\phi = \phi_0 [1 - 0.0337 \ln(1 + 0.6836 N^{3.3055})] \tag{15}$$

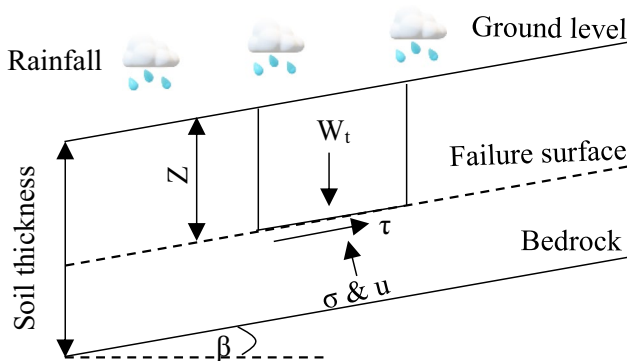


Fig. 5 Stability analysis of a shallow infinite landslide

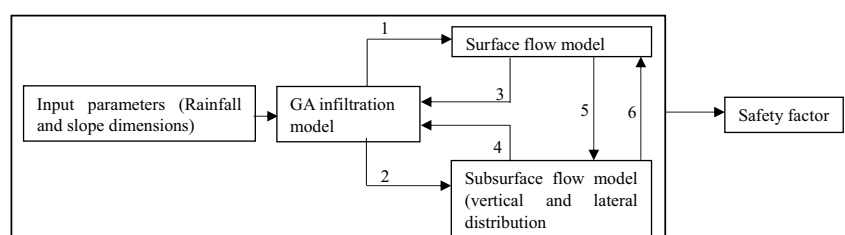
where  $c$  is the degraded cohesive force;  $c_0$  is the initial cohesive force;  $\phi$  is the degraded angle of internal friction;  $\phi_0$  is the initial angle of internal friction values; and  $N$  is water–rock interaction times.

Previous academics have noted that the location and size of shallow landslides are influenced by the spatial variation in geotechnical properties of the soil, the thickness of the unstable layer, topography, duration and intensity of rainfall, and the hydraulic transient condition of the soil. Previous rainfall zonation maps are not suitable for use as a dynamic tool that changes over time. Therefore, choosing dynamic maps as an option will be favorable to saving infrastructure, warning humans, and taking probable actions to save the economy (Valentino et al. 2014). Thus, a time-dependent model (SLIP-Shallow Landslides Instability Prediction) based on the limit equilibrium method and using the Mohr–column strength criterion (Valentino et al. 2014). This model accounts for saturated and partially saturated hydro geotechnical processes. Additionally, it correlates the factor of safety with rainfall amount, including previous rainfall. The SLIP model is a transient hydrological model that considers vertical and horizontal flow, unlike TRIGRS, which assumes that infiltration and the change in pore water pressure are in the vertical dimension based only on the analytical solution of Richard’s equations. Thus, the SLIP model accounts for the destabilizing filtration model, as TRIGRS does not consider these forces. The failure mechanism can be illustrated as follows: in full saturation, the pore water pressure can increase due to rainfall or water accumulation at a certain depth. In this case, the failure is due to decreased shear strength parameters. In partial saturation, soil can reach instability without being fully saturated due to the saturation of parts of the soil. Therefore, the failure surface can be above or at the soil–bedrock surface. The influence of nearby cells is taken into account since the unsaturated zone might be impacted by the adjacent saturated region, which in turn influences the stability of a catchment. Thus, sliding will occur when a relatively wide continuous stratum of saturated soil has formed. It should be noted that the model is affected by an effective rainfall amount due to the evaporation and runoff process. Runoff depends on the existing soil moisture at the time of the rainfall event.

Considering the most recent model, accurate prediction mainly depends on the actual initial conditions. (TAG-FLOW) the three surface regimes (infiltration, runoff, and exfiltration) can be identified to imitate the real initial conditions. To ease the computational challenges of the Richard equation, a model (TAG-FLOW) was constructed in Fortran 90 (Thang et al. 2022). The modelling process is presented in Fig. 6. Based on the Mohr–Coulomb law, this model assumes an infinite slope that fails at the interface between shallow soil and bedrock substrate. The GA model estimates the slope surface’s infiltration capacity to separate infiltration and extra rainwater from precipitation. According to this model, the wetting front raises the groundwater level when it reaches that level. Simultaneously, the soil matric suction at the wetting front is set to zero to ensure complete saturation in the Green-Ampt model. However, lateral flow in the saturated soil layer, dependent on the hydraulic gradient, also causes the groundwater level to fluctuate. The groundwater exfiltration that occurs when the groundwater level reaches the ground surface at any site combines with any excess rainfall there to create surface water on the ground surface. It is concluded that either subsurface flow or surface flow controls the landslides. Like available numerical models, TAG-FLOW is highly dependent on initial conditions that require a massive effort to be collected for a wide catchment. TAG-FLOW prediction slightly outweighs the TRIGRS model.

As a rule, it was essential to include geometrical conditions as input parameters, in addition to physical–mechanical and hydrological ones. This kind of large-scale operation, however, is difficult to do with an acceptable level of precision and uncertainty. One alternative approach to prediction is to look at the loading–unloading response ratio (LURR) (Wang et al. 2016). LURR is defined as the ratio of the loading to unloading reactions, and a quick rise suggests imminent failure (Yin et al. 1995). LURR is advantageous over previous studies as it is suitable for long-term triggered and deep-seated landslides. Zhang et al. (2006) adopted this theory between rainfall and landslide displacement. Wang et al. (2016) utilized this theory between the sliding force inside the slope as a load and unload parameter and displacement of the slope surface as

**Fig. 6** Schematic diagram of the modeling strategy



<sup>1</sup>Excess rainfall, <sup>2</sup>infiltrated rainfall, <sup>3</sup>pressure head, <sup>4</sup>suction head, <sup>5</sup>infiltration, <sup>6</sup>exfiltration

a response parameter. This technique, in contrast to available literature, takes into account solely internal factors and can be used for both shallow and deep-seated landslides. To clarify, this method can be used in case of insufficient data about rainfall or any external dynamic triggering factor (Wang et al. 2016).

Fluidized landslides and debris flows induce more severe damage than shallow landslides (Shu et al. 2016; Chae et al. 2020). The SHALSTAB model (Shu et al. 2016) and Debris 2D (Chae et al. 2020) can quantify this catastrophe based on different geomorphology and hydrology factors where the runoff distance mainly depends on the volume of debris and slope angle (Chae et al. 2020). This is out of the scope of this study.

### Numerical models

Previous analytical equations tried to simplify the complex equations using reasonable assumptions based on the initial conditions for a case study with a specific location. These models can only be generalized by considering real situations. Numerical analysis is time-consuming and costly, but it provides a more precise picture of the issue and can solve soil nonlinearity equations and complicated functions iteratively. Similar to analytical methods, numerical analysis is not recommended in large catchments (Huang and He 2023). Moreover, internal factors such as topographic, geological, geotechnical, and hydrological factors can be considered.

Numerical models have several advantages compared with analytical models, which can be mentioned as follows: 1) These models can consider various triggering factors such as rainfall (Calvello et al. 2009; Das et al. 2022; Huang and He 2023), reservoir level fluctuation (Li et al. 2021; Wan et al. 2017; Xu et al. 2022), earthquakes (Yang et al. 2023), and energy provided by high waves (Hobbs et al. 2020) where these factors can be separated or combined; 2) They include complex geometry such as deep soil depth, steep gradients, and material anisotropy (Liang and Uchida 2022); 3) They include virtual monitoring points that replicate the real monitoring locations in the slope considering the three-dimensional impacts that may affect slope seepage and stability during rainfall infiltration (Qiu et al. 2019); 4) They consider the delayed rainfall peak pattern effect (Liang and Uchida 2022); 5) They reflect the effective stress due to volumetric water content and the influence of dead weight under the effect of rainfall (Qiu et al. 2019); 6) They can overcome the problem of unmonitored physical characteristics using back analysis of the available data (Abolmasov et al. 2015; Li et al. 2021); 7) They consider the change in failure mechanism using full model geometry instead of the soil–bedrock interface assumptions (Li et al. 2021); 8) They can consider some asymmetric factors such as a surcharge

on slope crest that can reduce the stability of 3D slopes (Sun et al. 2022; Purnama et al. 2022); 8) They can build a parametric study to create various relationships (i.e., the relation between shear strength ( $\tau$ ), shear stress ( $\sigma$ ) and slope angle ( $\beta$ ) on the factor of safety) (Khan and Wang 2021); 9) They consider various analytical techniques for example Bishop simplified, Corps of Engineers #1, Corps of Engineers #2, GLE/Morgenstern-Price, Janbu simplified, Janbu corrected, Lowe-Karafiath, Ordinary/Fellenius, and Spencer method, which are available in the limit equilibrium program, SLIDE (Khan and Wang 2021); 10) They combine both seepage analysis (i.e., infiltration, evaporation, runoff) with slope stability analysis (Das et al. 2022); 11) They consider the nature of the bedrock layer, which can delay or decrease the failure time (Pagano et al. 2010); 12) The factor of safety against time considering hydro-fluctuation can be analyzed (Wan et al. 2017).

A comparison between dynamic and steady-state hydrological models was utilized to prove this. Liang and Uchida (2022) adopted the H-SLIDER (hillslope-scale shallow landslide-induced debris flow risk evaluation) method based on Darcy's law (Uchida et al. 2009) model as a steady-state model to calculate the factor of safety and critical rainfall. Then, a comparison is made with the finite element method to solve the three-dimensional Richards equation for a small catchment considering shallow rainfall-induced landslides. Steady-state hydrological models provide a simple approach based on Darcy's law or topographic-driven wetness. In contrast, dynamic models represent time-varying groundwater responses to rainfall intensity and can be described based on kinematic wave equations or Richards equations. It is important to note that the dynamic model illuminates the delayed rainfall peak pattern effect that is not considered using a steady model. In addition, steady models underestimate the number of unstable locations relative to dynamic methods. Dynamic models provide double-precision considering deep soil depth and steep gradients than steady models, while the steady model is better for predicting large areas (Liang and Uchida 2022).

A wide range of literature neglects the horizontal flow, considering only the isotropic vertical flow of water because the horizontal flow is slower than the vertical flow. The assumption mentioned above leads to overestimating the safety factor (Formetta and Capparelli 2019). Thus, considering the prototype's complex initial condition, a new method does not theorize any potential future surface using GEOTop 2.0 as a hydrological model. This high-resolution distributed water and energy budget model considers flows of variably saturated soil, snow cover dynamics, soil freezing, and terrain effects. This model uses a full three-dimensional description of the Richard equations. This model calculates the combined effect of various anisotropy ratios and replicates the dynamics of soil moisture as well as the shapes (convex, concave, and planar) on the stability of

slopes. Increasing the anisotropy results in a decrease in the duration before failure. Convex morphologies have a wider unstable area than planar and concave morphologies.

Landslide prediction can be analyzed based on the maximum movement velocity and displacement scenarios using the commercial finite element transient groundwater model SEEP/W (Geo-Slope 2004) (Calvello et al. 2009). To illustrate, the time-dependent changes in groundwater pressures control the landslide movements. The landslide starts to move, accelerate, or stop based on the groundwater pressure fluctuation. A creep threshold above which displacement occurs based on the residual strength envelope in the Mohr-Coulomb plan is presented in Eq. 16. The effective normal stress on the slip area is calculated, assuming that the only variable with time is porewater pressure (Eq. 17). Finally, the safety and creep displacement factors varying with time are computed (Eqs. 18 and 19, respectively) (Calvello et al. 2009).

$$\tau_{creep} = \sigma'_{slip} \tan(\phi'_r) \tag{16}$$

$$\sigma'_{slip} = (\gamma_{sat} \cdot H \cdot \cos^2 \beta - u(t)) \tag{17}$$

$$F(t) = \frac{(\gamma_{sat} \cdot H \cdot \cos^2 \beta - u(t)) \tan \phi'_r}{\gamma_{sat} \cdot H \cdot \sin \beta \cdot \cos \beta} \tag{18}$$

$$v_B = B \cdot (1/F(t))^{n_v} \tag{19}$$

where  $\sigma'_{slip}$  is the effective normal stress on the slip surface;  $\phi'_r$  is the residual friction angle of the soil within the deep creep zone; B represents the constant of the typical velocity of the phenomenon; and  $n_v$  constant represents the variation of viscosity with the excess shear stress.

Based on the mathematical equations, the innovative critical curve model of the rainfall intensity – time required to form the shallow saturated zone is established and calculated. ABAQUS software using a CPE4P element in a quadrate shape is used as a numerical model assisting in infiltration analysis (He et al. 2021). Equation 20 presents the relationship between rainfall intensity and hydraulic conductivity, considering the slope angle and depth of the infiltration layer. The SWCC can be accurately defined by Mualem-van Genuchten (MVG) (Schaap and van Genuchten 2006). The critical curve is used to predict landslides through the saturated zone and is developed based on a piecewise function (Eq. 21 and Fig. 7) (He et al. 2021).

$$I \cos \beta = K_{sat} \left[ 1 - (1 - S_e)^{\frac{1}{m}} \right]^2 S_e^{0.5} \tag{20}$$

$$I(t) = at^{-b} + c(t < t_c) \\ = I_c(t \geq t_c) \tag{21}$$

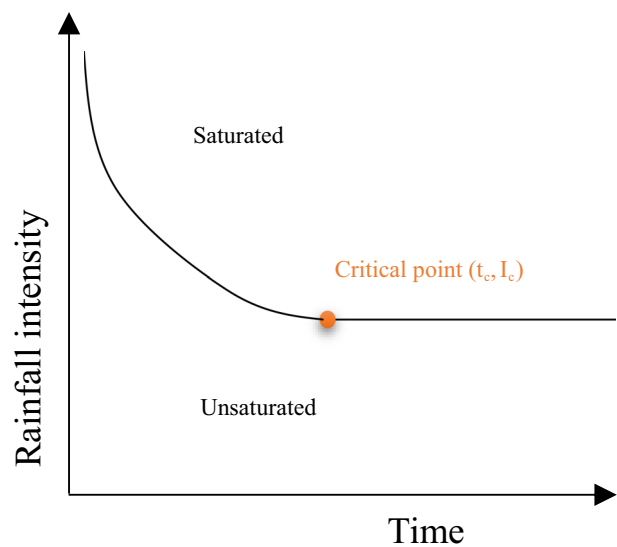


Fig. 7 The critical curve of rainfall intensity – time

where  $S_e$  is the effective saturation; I is the rainfall intensity; a and b are the fitting parameters; and c is the correction coefficient.

Three categories of numerical analysis models are available: large deformation analysis, small deformation analysis, and non-deformable analysis. In other words, numerical modeling can be categorized to be pre-failure analysis (limit equilibrium analysis and finite element analysis) and post-failure analysis (large deformation analysis). Limit equilibrium analysis (LEA) can be used to study the non-deformable (uncoupled) analysis. The LEA methods are single free body methods (i.e., infinite slope, log spiral, and Swedish circle) or multiple free bodies (Fredlund and Krahn 1977) (i.e., ordinary method of slices (Fellenius, 1936), simplified Bishop’s method (Bishop 1955), Spencer’s method (Spencer 1967), Morgenstern and Price’s method (Morgenstern and Price 1965), Duncan’s method (Duncan 1996), Chen and Morgenstern’s method (Chen and Morgenstern 1983), and Sarma’s method (Sarma 1987)). LEA ignores soil deformation by assuming only seepage analysis and does not account for variations in vertical and shear stresses caused by pore water pressure variations (i.e., consider only the weight of the slice) (Feng et al. 2023; Nguyen et al. 2019; Oliveira et al. 2022). Coupled analysis (small deformation finite element analysis) considers both seepage and soil deformation over time (Matyas and Radhakrishna 1968; Sitarenios et al. 2021; Cuomo et al. 2021; Postill et al. 2021; Song et al. 2020; Tang et al. 2019). However, this type of analysis is more complex and requires computational power compared with LEA. In large deformation, finite element analysis suffers from mesh distortion. The hydro-mechanical coupled process is seldom taken into account when forecasting landslides

(Zhang et al. 2011). Large deformation analysis (fully coupled analysis) has been used recently by some researchers (Cuomo et al. 2021; Liu et al. 2020; Yamaguchi et al. 2023; Zhu et al. 2022; Lee et al. 2021). Large deformation analysis can be handled by several methods, including the Material Point Method (Cuomo et al. 2021), Particle Finite Element Method, Finite Element Method with Lagrangian Integration Points, Smooth Particle Hydrodynamics, and Coupled Eulerian–Lagrangian methods (Chen et al. 2019). However, such models are hugely time-consuming and sometimes unfeasible as they are implemented in explicit schemes that necessitate small time steps (Yerro et al. 2022). This study focuses on pre-failure prediction, for post-failure prediction please refer to the review papers by Soga et al. (2016) and Yerro et al. (2022).

### Combined models (probabilistic and artificial intelligence with physical models)

Most researchers have adopted physical models considering the local scale and fixed values for input parameters. Multiple studies have merged physical models with landslide susceptibility maps to take advantage of the physical model's accuracy. Due to a lack of input data related to time-varying rainfall, topography, soil thickness, initiating water table depth, material strength, and hydraulic characteristics, these models will likely experience significant uncertainty. Thus, model calibration is a critical component in deploying physical-based models. Uncertainties in loadings, soil qualities, other factors, computational models, and human actions are among the uncertainties in slope engineering. The soil is a naturally occurring substance created by complicated geological processes resulting in significant uncertainty in the spatial variability of soil characteristics. Therefore, the probabilistic analysis offers a viable way to overcome this limitation, such as utilizing Monte Carlo simulation (Huang and He 2023; Salvatici et al. 2018; Wu et al. 2015) and employing logistic regression (Chae et al. 2020). However, statistical measures such as the mean, standard deviation (STD), and probability density function (PDF) for random variables adequately reflect the data properties when used in the probabilistic analysis approach. Therefore, the reliability of the probabilistic analysis would suffer if these statistical parameters were wrong. Nevertheless, due to time constraints, site accessibility issues, and budget constraints, landslide susceptibility studies are typically conducted across a large region, making

it challenging to acquire enough data to analyze the statistical characteristics appropriately. As a result, the lack of sufficient information limits the determination of precise statistical parameters for random variables, which would negatively impact the probabilistic analysis's dependability. Depina et al. (2020) considered the spatial uncertainty of physically based model parameters using the Bayesian framework to overcome such issues. Ji et al. (2022) used Python programming and the GIS-FORM landslide prediction toolbox.

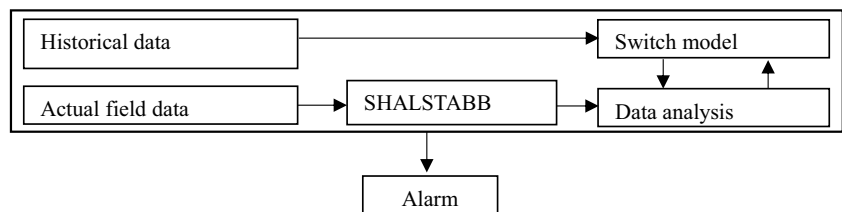
Liu et al. (2022) utilized a slope digital twin model that is updated in real-time to account for temporal variations in landslide stability and to minimize uncertainty. Bayesian probabilistic back analysis is used to update the slope model while accounting for various slope model uncertainties. Hwang et al. (2023) utilized the bootstrap and point estimation methods to consider the uncertainty coming from limited information on spatially distributed soil material. The bootstrap-PEM method can provide better results than the Monte Carlo (MC) simulation method. Oguz et al. (2022) developed the 3-dimensional probabilistic landslide susceptibility (3DPLS) for assessing landslide susceptibility to account for the three-dimensional effect of slope stability. This model surpasses the Monte Carlo simulation model, while the MC model has better performance regarding computational time and memory. The probability of failure,  $P_f$ , for each cell individually is calculated as follows (Eq. 22):

$$P_f = P(F_s \leq 1.0) = \frac{1}{N_s} \sum_{i=1}^{N_s} IF(F_s, i - 1.0) \quad (22)$$

where  $N_s$  is the number of simulations;  $F_{s,i}$  is the factor of safety of  $i^{\text{th}}$  simulation; and  $IF$  is the indicator function providing 1 in case of failure, when  $F_{s,i} \leq 1$ , otherwise 0.

Artificial models lack accuracy, while physical models suffer from complexity. Thus, it is proven that by reasonable training, artificial models can provide good accuracy (Utomo et al. 2019; Marrapu et al. 2021). A new model called the model switch-based landslide prediction system (MoSLaPS) was proposed by Utomo et al. (2019). This model can overcome the drawbacks of ANN models that cannot predict the pattern of the minority class. The newly proposed model can predict the occurrence of a landslide 44.2 min before the event. MoSLaPS consists of 1) a physically based model SHALSTAB to calculate the factor of safety based on geotechnical, environmental, and geological data; 2) an adaptive

Fig. 8 MoSLaPS flowchart



synthetic sampling (ADASYN) method to solve the imbalanced data; and 3) an ANN model to switch and train the model (see Fig. 8). This model is compared with the BPNN, SVM, and AdaBoost models. All models have an accuracy greater than 90%; however, the best model should achieve the highest TPR and the lowest FPR, which was achieved by the MoSLaPS model (98.40% and 2.01%, respectively). BPNN, SVM, Adaboost, and MoSLaPS achieved an accuracy greater than 90% due to a well-established dataset that considers the physical properties (Utomo et al. 2019).

Unlike Utomo et al. (2019), who employed the simple physical model to construct their model, Marrapu et al. (2021) built extensive data of 15,000 datasets that account for more complex features. ANN was used to train the above-mentioned comprehensive datasets of the following features: slope geometry (height and slope), shear strength parameter (cohesion, internal friction angle, and density), and factor of safety. The Michalowski stability chart method developed the stability analysis, which is verified with the numerical model Geostudio (2012) software (Bishop method). One of the major advantages of this study is that using an ANN trained with an extensive dataset can be applied to any other region, unlike all previous models that can only represent regional areas. The factor of safety of the ANN with comprehensive training data achieved the best accuracy compared with the ANN with limited data according to the MSE, RMSE,  $R^2$ , and VAR values (0.010, 0.099, 0.987, and 98.716, respectively).

Dai et al. (2022) proposed a unique model that can provide perfect accuracy by merging numerical analyses with deep learning models. This methodology overcomes the uncertainties of geotechnical parameters using the displacement back analysis technique (DBA). The horizontal and vertical GNSS surface displacements in DBA were assigned in the input layer. At the same time, the modified geotechnical factors (modified cohesion and internal friction angle) were the output of the LSTM model. LSTM can increase the effectiveness of back calculations and substitute for time-consuming numerical simulations. Then, numerical modeling can be run based on the modified parameters using the tension–shear damage strength reduction method (Wang et al. 2014). Not only can a numerical model analyze the slope, but it can also provide failure thresholds (Zhang et al. 2023). The DBA-LSTM was compared with DBA-BPNN, and the MAPE was 0.62% and 1.63%, respectively. Moreover, it utilized a unique dataset extracted from the verified numerical model for perfect prediction of the factor of safety using the deep learning LSTM model.

#### Discussion of deterministic models (advantages, assumptions, and limitations)

Physical models have numerous advantages: Accurate prediction can be obtained by considering the infiltration and seepage process, actual stress, and deformation under different dynamic

factors such as rainfall, earthquake, and reservoir level fluctuation. Numerical models provide a viable tool for considering such complex behavior and identifying the actual complex initial conditions. Physically based models are dependable, effective, and accurate tools in cases of rainfall-induced landslide evaluation. However, higher accuracy is needed in evaluating input geotechnical parameters, particularly regarding the influence of shear strength parameters (Bicocchi et al. 2019; Valentino et al. 2014). Furthermore, these models demand extensive geotechnical work that is not readily available.

In some cases, while reasonable assumptions can be made, analytical analysis can simplify the complexity of the initial conditions. Considering the infinite slope analysis, the limit equilibrium method can be used to calculate the factor of safety. The area can be divided into grids of cells in the GIS framework. The stability of each cell can be obtained considering the neighboring effect. The input data for each cell or model can be summarized as follows: 1) topographic data such as elevation and slope; 2) geotechnical data such as soil profile, initial water condition, and soil properties; 3) hydrological properties; and 4) triggering factors such as rainfall patterns. The factor of safety corresponding to time-varying pore water pressure can be developed, as  $FS > 1$  indicates a stable slope or no landslides, and  $FS < 1$  indicates that the slope is unsafe or there is a landslide.

Some limitations of the current research can be illustrated as follows: It is seen that coupled analysis is not widely used as the complexity of the landslide mechanism is simplified to be a seepage problem neglecting soil deformation which may be misleading in terms of temporal and spatial prediction. The weathering effect (i.e., the randomness of the rainfall pattern) is not widely considered (Postill et al. 2021). The influence of groundwater chemistry is disregarded in this case. For instance, when rainwater seeps into a landslide, several gases dissolve in it and cause a higher level of chemical aggression. This will amplify the porosity and permeability of the soil. Rock weathering is another effect. As a result, the physical characteristics of the soil will change.

#### Landslide susceptibility maps

Landslide susceptibility, risk, and vulnerability maps are crucial for land use, development, and planning. Susceptibility maps can be defined as the likelihood of landslides occurring in a specific location where risk is not properly quantified as the time is not expressly considered (Fell et al. 2008; Corominas et al. 2023). Landslide risk maps classify the areas of the ground surface based on the risk of landslides or other mass movements on slopes, either actually or potentially, within a given period (Corominas et al. 2023). Therefore, these additional data are used to quantify the risk, such as landslide volume, material involved, type

of movement, and depth of failure surface (Anbalagan et al. 2015; Bezerra et al. 2020; Riaz et al. 2023; Pecoraro et al. 2023). The term "vulnerability" refers to the range of consequences that follow the effect of the landslide on the exposed element or elements (Corominas et al. 2023). Vulnerability assessment refers to the severity of loss for objects that are at risk (Shah et al. 2023). It necessitates more information on the probable damage to the local population, economy, and property. In this section, the landslide susceptibility for shallow landslides is discussed. Figure 9 represents the flowchart for landslide susceptibility mapping. The analysis process can be summarized in six steps: landslide inventory and controlling features; landslide event-based and sampling ratios; model selection; landslide maps; and evaluation of the model. Each process will be discussed briefly in the following lines.

### Data inventory, controlling features, and landslide event maps

An important first step to enhance the accuracy of predictions is data inventory. Satellite images, geological maps, digital elevation models, aerial photographs, maps of rock-mass structure, maps of rock strength, maps of roads, recordings of site monitoring, historical datasets, reports from governments, publicly accessible spatial data, and so on may all be used to compile data inventory. Nevertheless, the precision and detail of such data are of utmost importance in order to minimize the impact of any background noise on the predicted model's accuracy. The source of data is related to landslide monitoring techniques and will be further discussed in future research. Data inventory can be mapped using GIS. Afterward, more than 50 different factors can be extracted (Yang 2017). Generally, the factors can be defined as creep features combined with external triggering or dynamic factors. Creep features have almost minimal change with time. At the same time, the most affecting parameters are dynamic,

such as rainfall (Hu et al. 2019), earthquakes (Hu et al. 2013), reservoir level fluctuation (Hua et al. 2021), and change in land use (i.e., infrastructure project developments) (Yu et al. 2023). Figure 10 presents the causative feature classification (Varnes 1984). However, based on the available data and initial conditions, each case study has its key features, which will be further discussed in the following lines for each case study (Table 4).

Inventory maps can be categorized as spatial maps (Al-Batah et al. 2015; Dang et al. 2019; Guo et al. 2022; Hanafiah et al. 2019; Hu et al. 2019, 2013; Kainthura and Sharma 2022; Karim et al. 2019; Liao and Dennis 2004; Manchar et al. 2018; Midhuna et al. 2022; Oh and Lee 2017; Selamat et al. 2023; Sharma and Mahajan 2018; Tengtrairat et al. 2021; Tien Bui et al. 2017; Wang et al. 2009; Wang and Niu 2010; Wubalem 2021; Wubalem et al. 2022; Yang et al. 2022; Yang 2016, 2017; Zhu and Huang 2006), dynamic (Hua et al. 2021; Yu et al. 2023), and spatiotemporal maps (Collini et al. 2022; Harsa et al. 2023; Mondini et al. 2023; Ng et al. 2021; Shano et al. 2021; Xiao and Zhang 2023; Xiao et al. 2022). Spatial maps may be defined as the geographic likelihood of occurrence of landslides depending on a set of geo-environmental parameters. An effective way for spatially analyzing landslide susceptibility maps is to use GIS and similar data inventory sources. Dynamic maps present the change in landslide susceptibility with time with the rapid change in land use. Spatiotemporal maps represent the chance of landslide occurrence during a certain era (when) and area (where). Thus, after extracting and assigning the causative factors using GIS, event-based landslide maps can be established by comparing pre-event and post-event maps.

### Feature weighting, optimization, and model analysis

Landslide susceptibility maps can be classified into direct (qualitative) and indirect (quantitative) maps. Figure 11

**Fig. 9** Landslide susceptibility mapping flowchart

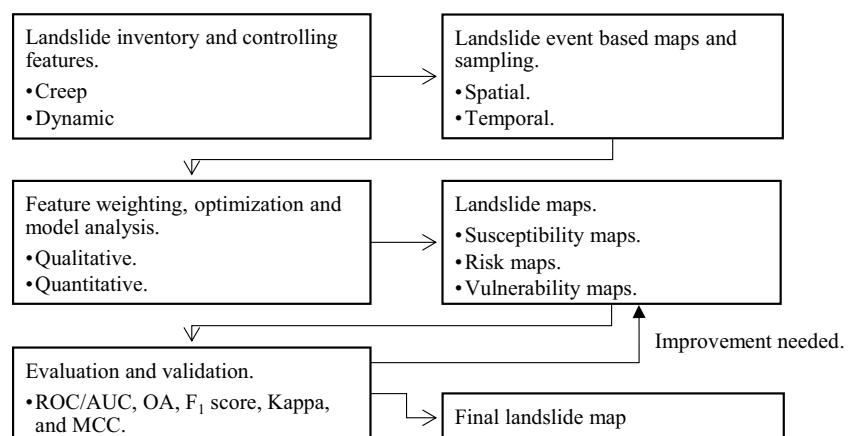
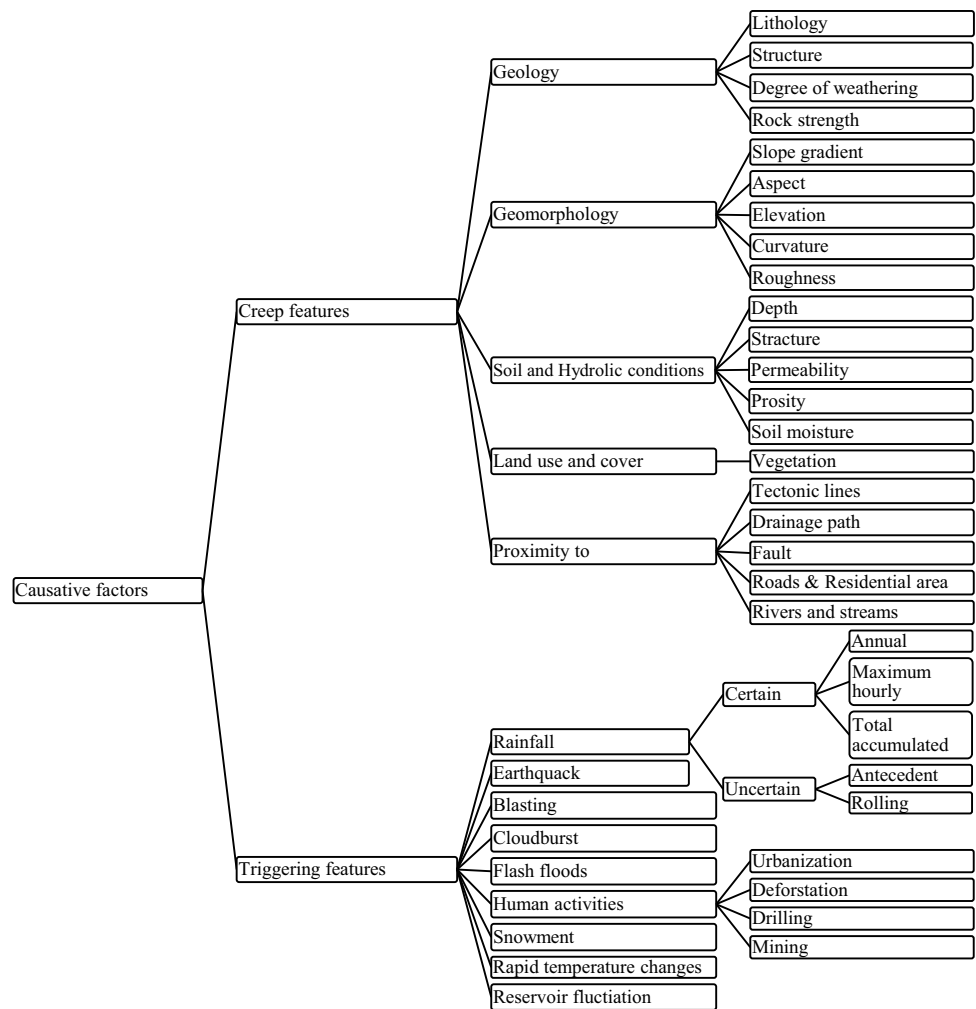


**Fig. 10** Causative feature classifications



illuminates the sequence and classification of different methods. For more refinement, Fig. 12 highlights different intelligence models, and each method will be further discussed in the following subsections.

**Qualitative models**

Direct mapping is mainly pertinent to historical landslides and experts' experience. These maps are subjective or qualitative, or semi-quantitative processes such as the analytic hierarchy process (AHP) (Hanafiah et al. 2019; Sharma and Mahajan 2018; Zangmene et al. 2023) weighted linear combination (WLC) (Liao and Dennis 2004), and fuzzy logic (FL) (Wang et al. 2009). The limitation of the qualitative method is that its accuracy depends on the knowledge of the experts conducting the investigation. However, quantitative methods examine the correlation between landslides and triggering factors to predict the likelihood of their occurrence by weighting landslide contributory variables.

**Quantitative models**

Indirect mapping includes a statistical analysis of numerous features controlling landslide occurrence. Indirect mapping can be classified as bivariate, multivariate, and intelligence analysis models to investigate the relationship between landslide-controlling features and spatial susceptibility. These models are quantitative approaches.

**I. Bivariate and multivariate models** Bivariate models compare the landslide-controlling feature maps with the inventory maps to classify the function of each feature regarding landslide occurrence. These models include information value (IV) (Karim et al. 2019; Manchar et al. 2018; Wubalem 2021; Wubalem and Meten 2020), frequency ratio (FR) (Karim et al. 2019; Manchar et al. 2018; Midhuna et al. 2022; Wubalem 2021; Wubalem et al. 2022), weight of evidence (WoE) (Karim et al. 2019; Manchar et al. 2018), certainty factor (CF) (Wubalem 2021), and index of entropy (IOE) (Wubalem et al. 2022). These approaches are simple

**Table 4** Recent contribution toward landslide susceptibility maps

Study	Key Features	Susceptibility map		Model with the best accuracy	Sampling ratio (training: testing)	Model performance % AUC <sup>1</sup> , PPV <sup>2</sup> , ACC <sup>3</sup> , K <sup>4</sup> , MCC <sup>5</sup>	Notes
		Spatial	Temporal				
Spatial maps: (Zhu and Huang 2006; Wang et al. 2009; Wang and Niu 2010; Yang et al. 2012, 2022; Hu et al. 2013, 2019; Al-Batah et al. 2015; Yang 2016, 2017; Oh and Lee 2017; Tien Bui et al. 2017; Man- char et al. 2018; Sharma and Mahajan 2018; Karim et al. 2019; Dang et al. 2019; Hanafiah et al. 2019; Wubalem and Meten 2020; Wubalem 2021; Long et al. 2021; Tengtrairat et al. 2021; Midhuna et al. 2022; Wubalem et al. 2022; Shano et al. 2021; Guo et al. 2022; Kainthura and Sharma 2022; Selamat et al. 2023; Ikram et al. 2023)	Creep: elevation, gradient, aspect, distance to roads, rivers, faults, streams, and residential area, lithol- ogy, geomorphology, land cover, groundwater, topographic wetness index (TWI), timber age, normalized difference veg- etation index (NDVI), land use, and relative relief Dynamic: Current, rolling, and antecedent rainfall data, reservoir level fluctuation, and land-use change	√	-	TFNW AHP DA WoE FR LR IV CF IoE ANN BPNN (MLP) BT RFC SFO-MLP COA-MLP CFNN-LM LSSVM-BC SOM-RF MLP-FR LMT-RF DM-chameleon Bi-LSTM-FR	- Varied sampling ratio (please see Section "Sampling ratio") - 70%:30% is widely adopted	- 78.0 <sup>1</sup> 83.6 <sup>1</sup> 79.09 <sup>1</sup> 88.83 <sup>1</sup> 84.4 <sup>1</sup> 88.6 <sup>1</sup> 87.03 <sup>1</sup> 74.5 <sup>1</sup> 95.7 <sup>1</sup> , 92.9 <sup>3</sup> , 0.86 <sup>4</sup> , 95.2 <sup>2</sup> 81.285 <sup>2</sup> , 871, 88.50 <sup>3</sup> 90.79 <sup>1</sup> 92 <sup>1</sup> , 80.78 <sup>3</sup> 71.9 <sup>1</sup> 79.7 <sup>1</sup> 77.62 <sup>1</sup> 98.4 <sup>1</sup> 91.4 <sup>1</sup> , 91.36 <sup>1</sup> 97.19 <sup>1</sup> 89.7 <sup>1</sup> 82.50 <sup>3</sup> , 0.888 <sup>4</sup> 100 <sup>1</sup> 98.1 <sup>1</sup> , 95.74 <sup>2</sup> , 98.1 <sup>3</sup> , 0.901 <sup>4</sup> 99.5 <sup>1</sup> , 97.93 <sup>2</sup> , 99.5 <sup>3</sup> , 0.941 <sup>4</sup> 86.0 <sup>1</sup> , 0.2432 <sup>6</sup> 90 <sup>1</sup> 94 <sup>1</sup> 99 <sup>1</sup> , 99 <sup>3</sup> , 0.27 <sup>4</sup> , 33 <sup>2</sup> 82.6 <sup>1</sup> 83.6 <sup>1</sup> 88 <sup>1</sup> , 78.3 <sup>3</sup>	- Trapezoidal fuzzy number weight- ing (TFNW) has the advantage of combining both expert and statistical weighting of the controlling features of landslide occurrence - Random forest classifier (RFC) can consider the non-linearity and overfit- ting phenomenon - Least squares support vector machines (LSSVM) and artificial bee colony (ABC) were utilized to overcome the shortening of the SVM. LSSVM is a modified SVM that can deal with complex parameters - SOM-RF model applies the under- sampling method to approximately equal the number of non-landslides with the number of landslides to solve the problem of unbalanced sampling - The MLP presents better discre- tization criteria. To illustrate, data discretization can result in a big difference between two samples in the same category - MLP-FR as a hybrid model outper- forms MLP and FR as a single model - LMT combines the merits of decision trees and logistic regression models that avoid the problem of overfitting - The DM-chameleon can identify the clusters that the M-chameleon cannot - DNN is more competitive in depict- ing a complex nonlinear problem - Selecting controlling features has equal importance to selecting the algorithm as RF, LR, and SVM can achieve better results
Dynamic maps: (Hua et al. 2021; Yu et al. 2023)				DNN RF ANN			
Spatio temporal maps: (Ng et al. 2021; Xiao et al. 2022; Collini et al. 2022; Xiao and Zhang 2023; Harsa et al. 2023; Mondini et al. 2023)			√	DNN RF LR CNN GLM DL DNN			

**Fig. 11** Statistical model classification

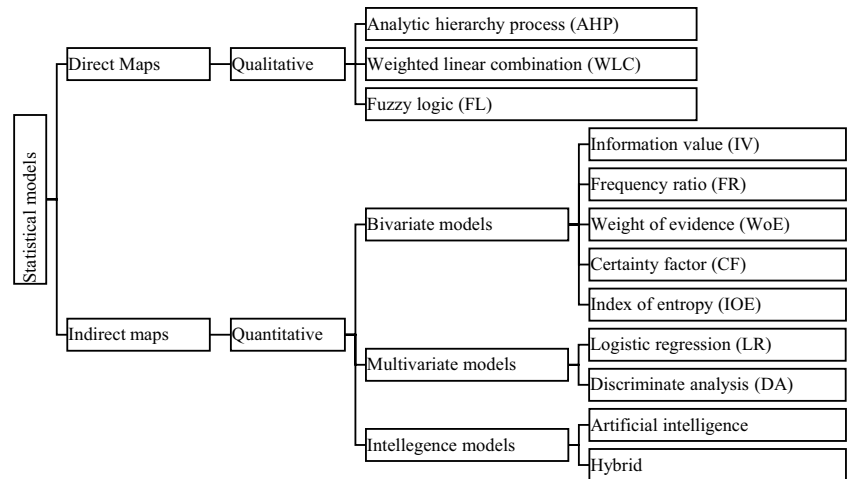
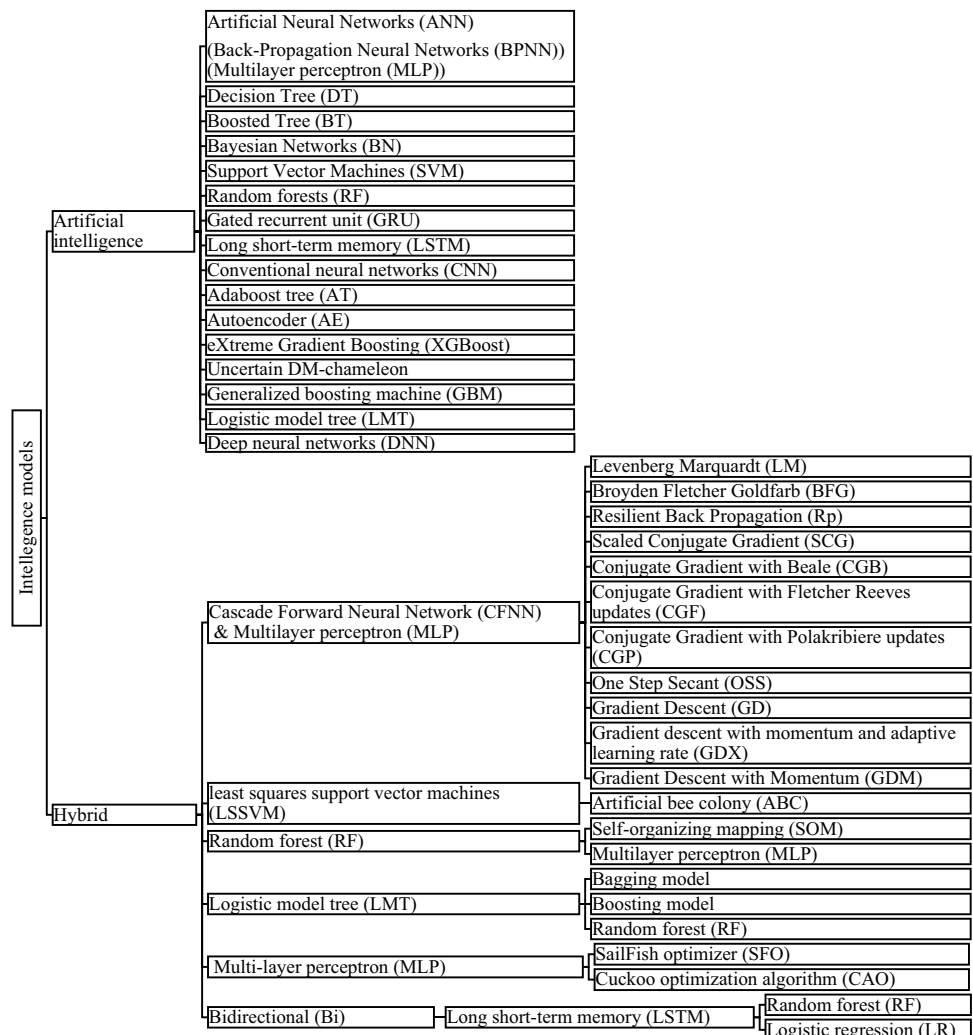


**Fig. 12** Intelligence model classification based on the database of this study



to implement but could be more reliable and have higher forecast accuracy.

However, the most adapted statistical models were multivariate models such as logistic regression models (LR)

(Dang et al. 2019; Hu et al. 2013; Karim et al. 2019; Ng et al. 2021; Shano et al. 2021; Wubalem and Meten 2020; Xiao and Zhang 2023; Yang et al. 2012; Yang 2016; Zhu and Huang 2006) and discriminate analysis (Dang et al. 2019;

Yang 2017). Multivariate models can be defined as those that explain the connection between the single or categorical response variable. These coefficients function as weights in an algorithm that may be applied to the GIS database to generate a map showing the likelihood that a landslide would occur. These models are fundamentally linear and need the creation of databases with information on the relevant environmental parameters and landslide occurrences. In contrast to bivariate techniques, the multivariate (LR) methodology cannot examine each component class's impact on landslide probability (Wubalem et al. 2022).

The widely used statistical models can be defined as follows: FR compares the landslide occurrence probability against the non-occurrence likelihood for a particular property. It is quick, easy, and used to assess the impact of each factor class. The IV model generates the weight for every element class by dividing the landslide density of a specific category by the overall area landslide density; however, this model cannot determine the controlling features (Wubalem and Meten 2020). The WoE derives prediction outputs from landslide occurrences as training points, considering the uncertainties associated with it. The log-linear from the Bayesian probability model is used in the WoE technique to determine the relative value of evidence by statistical means (Karim et al. 2019; Manchar et al. 2018). WoE has no assumptions for variable distribution. The certainty factor is one of the probabilistic approaches extensively used for mapping landslide susceptibility for various data (Wubalem 2021); LR computes the nonlinear relationship between the occurrence of landslides and the causative factors. This model can highlight the most dominant factors. At the same time, it mainly relies on historical landslides, as it assumes that past events will reoccur in the future, which can be considered a limitation.

**II. Artificial intelligence models** The "black-box" nature of intelligence and data mining models makes them accessible to anyone who may lack expertise in statistical analysis. When dealing with complicated and nonlinear interactions, these approaches are superior to regression models. In order to identify the multicollinearity issue, these models begin with a dataset containing all accessible attributes. With the rapid development of monitoring techniques and computer performance, geographic information systems (GIS), remote sensing techniques (RS), and global positioning systems (GPS) can be utilized in disaster analysis, providing enormous datasets. Thus, developing and applying advanced models to analyze these data is crucial. After analyzing the collected data to assemble information about landslide history and the key features related to factors, selecting intelligence techniques to use computational intelligence to calculate the probability of landslides began. Data mining techniques were recently developed and are incredibly useful

for dealing with a wide range of dynamic scenarios, such as artificial neural networks, decision trees, boosted trees, Bayesian networks, support vector machines, and random forests (Fig. 12). Such models tolerate ambiguity, imprecision, and imperfect actual values, have low cost, and are highly adaptable (Yanbin et al. 2022).

These models include single intelligence models: ANN (Oh and Lee 2017; Yu et al. 2023), BT (Oh and Lee 2017), DT (Wang and Niu 2010), MLP (BPNN) (Dang et al. 2019; Hu et al. 2013; Kainthura and Sharma 2022; Ng et al. 2021), RVMs (Dang et al. 2019), SVMs (Dang et al. 2019; Yu et al. 2023), (Ng et al. 2021), RF (Collini et al. 2022; Dang et al. 2019; Hua et al. 2021; Kainthura and Sharma 2022; Ng et al. 2021), GRU, and LSTM (Tengtrairat et al. 2021), CNN (Yu et al. 2023), (Collini et al. 2022), BN (Kainthura and Sharma 2022), Adaboost tree (Ng et al. 2021), AE (Collini et al. 2022), and XGBoost (Collini et al. 2022; Harsa et al. 2023), uncertain DM-chameleon algorithm (Hu et al. 2019), LMT model (Yang et al. 2022), GLM, DRF, and GBM (Harsa et al. 2023), and DNN (Harsa et al. 2023; Hua et al. 2021; Mondini et al. 2023). Recently, more advanced hybrid models were introduced to create a better model, such as CFNN with 11 different algorithms (Al-Batah et al. 2015), LSSVM-ABC (Tien Bui et al. 2017), SOM-RF, PCA-IE (Long et al. 2021), MLP-FR (Guo et al. 2022), LMT-RF, LMT-bagging model, LMT boosting model, LMT model (Yang et al. 2022), Bi-LSTM-RF, Bi-LSTM (Tengtrairat et al. 2021), COA-MLP, and SFO-MLP (Ikram et al. 2023).

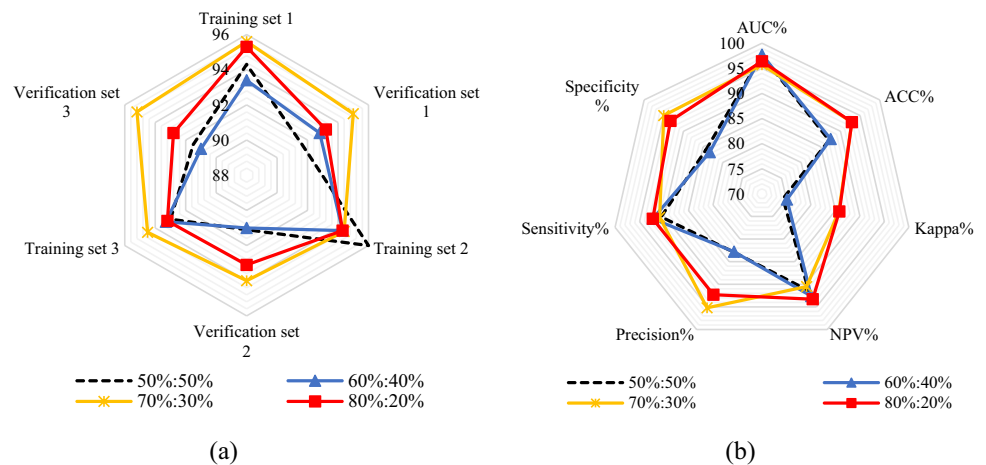
Merghadi et al. (2020) listed the theoretical background for most adopted machine learning models in landslide susceptibility. However, this study presents the most recent contribution in this field and deeply investigates the effect of different factors, initial conditions, model selection, and data preparation on prediction accuracy.

### Sampling ratio

The precision of the model relies significantly on the sampling ratio. There are three methods to adapt. The first is using data from the whole research region, resulting in an unequal number of pixels with landslide and non-landslide events. The second technique involves equal numbers of non-landslide and landslide pixels. However, the model's dependability may be lowered if it was built and verified using the same landslide data. The most sensible approach is to split the landslide pixels into training and test sets (Zhu and Huang 2006).

Hua et al. (2021) utilized different ratios (80%:20%, 70%:30%, 60%:40%, and 50%:50%) with different datasets, as shown in (Fig. 13-a). The 70% -30% ratio was almost stable with different datasets. Similarly, Selamat et al. (2023) investigated the most suitable sampling ratio using ANN

**Fig. 13** **a)** Model accuracy (AUC) with different datasets and different sampling ratios, **b)** Different accuracy metrics with different sampling ratios for the same dataset



using four sampling ratios (50%:50%, 60%:40%, 70%:30%, and 80%:20%), and the 80%:20% ratio achieved the best accuracy, followed by 70%:30%, 60%:40%, and 50%:50% ratios (Fig. 13-b). Ng et al. (2021) investigated the effect of different training ratios (50%, 60%, 70%, 80%, and 90%) with different models (LR, RF, ABT, SVM, and MLP). 70% achieved the best accuracy for RF, ABT, SVM, and MLP, while 60% recorded the best accuracy for LR. Hu et al. (2019) applied different testing samples (1%, 2%, 5%, 8%, and 10%), where 10% achieved better results. Zhu and Huang (2006) adopted all pixels in the training dataset due to the minimum amount of data, while the non-landslide pixels were selected randomly to overcome the issue of unequal proportions. Yang (2016) and Yang et al. (2012) utilized one rainfall event for training, while another rainfall event was used for model testing.

However, based on the current study, the ratio of 70%:30% is widely used (Guo et al. 2022; Hua et al. 2021; Karim et al. 2019; Long et al. 2021; Manchar et al. 2018; Ng et al. 2021; Shano et al. 2021; Wubalem 2021; Wubalem et al. 2022; Xiao et al. 2022; Yang et al. 2022; Yu et al. 2023; Ikram et al. 2023). This was followed by 80%:20% (Collini et al. 2022; Mondini et al. 2023; Selamat et al. 2023; Tengtrairat et al. 2021) and 75%:25% (Kainthura and Sharma 2022; Sharma and Mahajan 2018). Minor scholars proposed a 50%:50% ratio (Oh and Lee 2017), 66.67%:33.33% (Al-Batah et al. 2015), 78%:22% (Wubalem and Meten 2020), 74%:26% (Tien Bui et al. 2017), 60%:40% (Yang 2017), fivefold (Dang et al. 2019), and 20-fold (Harsa et al. 2023). Generally, the most adapted ratio was 70%: 30%.

**Performance metrics**

It is critical not only to select reliable factors and optimize features but also to cross-check and validate the model's dependability. The widely used performance value is AUC (refer to Fig. 14). AUC represents the area under the receiver operating characteristic (ROC) curve between

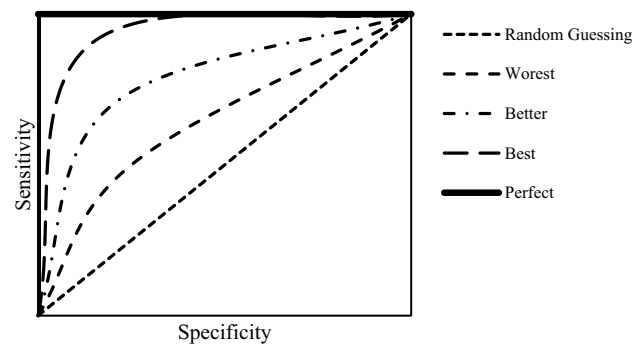


**Fig. 14** The receiver operating characteristic (ROC)

sensitivity and specificity. AUC ranges between 1 and 0. A value of 1 means that the model is perfect, and 0.5 means that the model behaves randomly as a coin toss. Likewise, the error matrix or confusion matrix is commonly adopted. An error matrix is a particular type of table arrangement that makes it possible to see how an algorithm performs (Table 2) (Stehman 1997). Six common performance metrics can be calculated: specificity, sensitivity (recall), accuracy (ACC) (classification accuracy rate-CAR (Dang et al. 2019)), positive predictive value (PPV) (precision), negative predictive value (NPP), and AUC can be calculated using Eqs. 23, 24, 25, 26, 27, and 28, respectively (Fawcett 2006). The  $F_1$  score (Eq. 29), which ranges from 0 (worst) to 1 (perfect), shows the harmonic median of the sensitivity and positive predictive value (Ng et al. 2021). The overall accuracy (OA) combines the accuracy,  $F_1$  score, and AUC (Eq. 30). The greater the OA is, the better the results (Ng et al. 2021). Matthew's correlation coefficient (MCC), where perfect prediction is represented by a coefficient of 1, average random forecast by 0, inverse prediction by a coefficient of -1 (Chicco et al. 2021), and

Kappa index ( $k$ ) nearest to 1 (Sim and Wright 2005), are presented in Eqs. 31 and 32, respectively.

FP and FN are the inaccurately recognized landslide or non-landslide occurrences; TP is the successfully identified landslide event; and TN is the correctly identified non-landslide event. P represents the total number of landslides, and N represents the total number of non-landslide events.

$$\text{Sensitivity} = TP / (TP + FN) \tag{23}$$

$$\text{Specitificity} = TN / (TN + FP) \tag{24}$$

$$\text{Accuracy} = (TP + TN) / (TP + TN + FP + FN) \tag{25}$$

$$PPV = TP / (FP + TP) \tag{26}$$

$$NPP = TN / (FN + TN) \tag{27}$$

$$AUC = \left( \sum TF + TN \right) / (P + N) \tag{28}$$

$$F_1 - \text{score} = 2 * (\text{recall} * \text{precision}) / (\text{recall} + \text{precision}) \tag{29}$$

$$OA = ACC + F_1 + AUC \tag{30}$$

$$MCC = \frac{TP * TN - FP * FN}{\sqrt{(TP + FP)(TP + FN)(TN + FP)(TN + FN)}} \tag{31}$$

$$k = (P_r(a) - P_r(e)) / (1 - P_r(e)) \tag{32}$$

where  $P_r(a)$  is the relative observed agreement, and  $P_r(e)$  is the hypothetical probability of chance agreement.

### Discussion of susceptibility models (prediction accuracy)

In order to assess the connection between various variables and the frequency of landslides, many statistical models have been developed. However, at this point, there has yet to be a consensus on which method is superior, although the general view is that each has strengths and drawbacks (Manchar et al. 2018). Nevertheless, the accuracy of such models depends on the quality of the monitored data, such as remote-sensing images (Yu et al. 2023). Previous Research has shown that by minimizing noise uncertainty, model prediction accuracy may be significantly improved through optimization and suitable feature selection (Shano et al. 2021; Wubalem et al. 2022; Yu et al. 2023). The sampling ratio also has a noticeable effect on the accuracy, as mentioned before (refer to Fig. 13) (Hua et al. 2021; Selamat et al. 2023). Hybrid algorithms also affect the accuracy of the model for

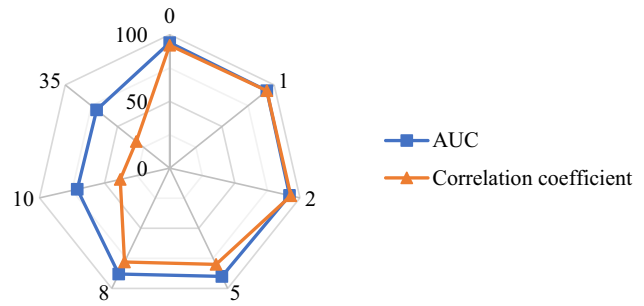


Fig. 15 AUC and correlation coefficient with observation frequency (years) of landslides

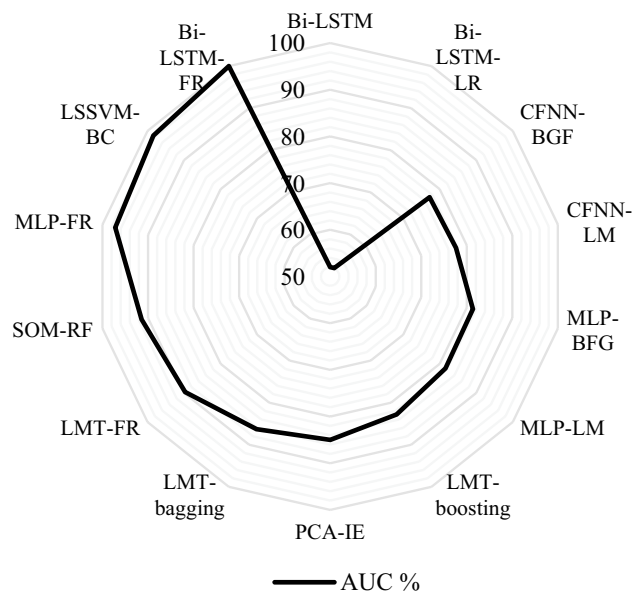


Fig. 16 AUC values for different hybrid models

the same dataset features (Al-Batah et al. 2015). Measuring the frequency of data affects the accuracy (Xiao and Zhang 2023) (please see Fig. 15). The quality of the dataset itself greatly affects the results. To prove this, the accuracy of LR and SVM was recorded at 88.52% and 91.88%, respectively (Hua et al. 2021). Thus, this emphasizes that the closer the dataset is to representing the actual initial conditions, the higher the accuracy of the model, even for simple models (Hua et al. 2021; Ng et al. 2021). The model may, therefore, be judged based on the information provided, the study's objectives, scalability, ease of use, speed, and capacity to deliver accurate findings (Wubalem et al. 2022). To clarify, there are two major issues: 1) choosing reasonable features based on a better understanding of the initial conditions of the case study, and 2) choosing a reasonable model to solve the relationship between such features. Table 4 represents the recent contribution toward landslide susceptibility maps,

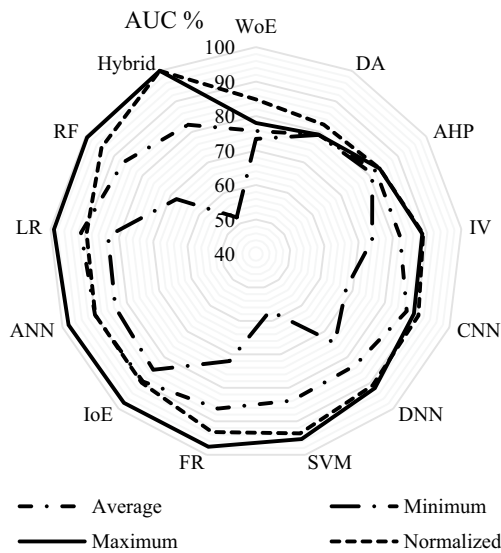


Fig. 17 AUC values for different statistical models

mentioning the causative features, selected model, sampling ratio, model performances, assumptions, etc. Figures 16 and 17 present a comparison between different models in terms of AUC%. Figure 16 illuminates the different hybrid models adopted for landslide susceptibility, where Bi-LSTM-FR, LSSVM-BC, and MLP-FR recorded the maximum AUC (100, 98.4, and 97.19, respectively). Figure 17 highlights the AUC for different statistical models in terms of maximum, minimum, average, and normalized AUC. Normalized AUC is measured as the ratio between the maximum AUC

divided by the average AUC for the same model as a percentage of the maximum value recorded to solve the issue of the different number of studies. WoE and DA recorded accuracies below 80%, followed by AHP, IV, and CNN, with values lower than 90%. RF and LR achieved an accuracy of 99%, while the other models recorded an accuracy between 92 and 98%, assuming a well-established dataset. The variance between the maximum and the minimum AUC for each model indicates the effect of other influencing parameters, which is shown in Table 4.

**Landslide susceptibility ranges**

The landslide susceptibility of each cell is measured by the landslide number ratio (LNR) or landslide susceptibility index (LSI), which represents the spatial distribution of the landslide occurrence probability. Landslide susceptibility ranges from 0% (non-landslide) to 100% (landslide). Generally, susceptibility maps are presented at different probabilistic levels. While no statistical function exists for such probabilistic categorization, expert opinion with available literature (please see Table 3) can be used (Ayalew and Yamagishi 2005; Yang 2017). Based on the current study, a five-fold classification (very low, low, moderate, high, and very high) is widely adopted (Dang et al. 2019; Guo et al. 2022; Hanafiah et al. 2019; Hua et al. 2021; Liao and Dennis 2004; Long et al. 2021; Manchar et al. 2018; Midhuna et al. 2022; Ng et al. 2021; Shano et al. 2021; Sharma and Mahajan 2018; Tien Bui et al. 2017; Wang et al. 2009; Wubalem 2021; Wubalem et al. 2022; Wubalem and Meten 2020; Xiao et al. 2022; Yang et al. 2022, 2012; Yu et al. 2023; Zhu and Huang

Table 5 Research gaps in landslide prediction models (Deterministic and susceptibility maps models)

Research Gaps	Recommendations
Consideration of the random effect of the rainfall pattern itself and the real-time monitoring of subsurface geotechnical characteristics needs to be improved. Constitutive modeling was required to account for internal changes in soil characteristics produced by triggering factors. Previous studies employed fixed values for soil characteristics or widely accounted for soil uncertainty using probabilistic and artificial intelligence models	It is recommended to provide real-time, multi-field (displacement, seepage, stress, etc.) and online observation with high-precision data to establish a real-time extensive dataset. There is a need to develop an advanced constitutive model to consider such complex behavior (i.e., the randomness of the rainfall events). Moreover, training an AI model with an extensive subsurface dataset helps predict such complicated mechanisms better
Considering the effect of chemical aggression is missing. In other words, when rainwater seeps into a landslide, several gases dissolve in it and cause a higher level of chemical aggression	The influence of groundwater chemistry shall be considered, as this will affect the porosity and permeability of the soil and may delay or accelerate the failure mechanism
Widely, prediction models were built based on the assumption that historical events will reoccur in the future, neglecting the change of features with time. However, rainfall is not the only dynamic factor; reservoir level, soil moisture, land use, and human activities can be considered dynamic factors that change with time	Implementing event-based maps and considering the dynamic change in the causal elements over time may aid in effectively detecting landslide susceptibility and avoiding inaccurate forecasts
Landslide susceptibility maps suffer high subjectivity (refer to Table 2)	A spatiotemporal susceptibility map based on the actual mechanism of the slope (i.e., the safety factor) may overcome the limitation of such subjectivity
The effect of the initial conditions, key features, sampling ratio, observation frequency, dataset, and model selection on the AI prediction accuracy for susceptibility maps still needs research	A sensitivity analysis considering several AI models, different sampling ratios, and data rates assists in selecting the optimum model and best data set that may help achieve higher prediction accuracy

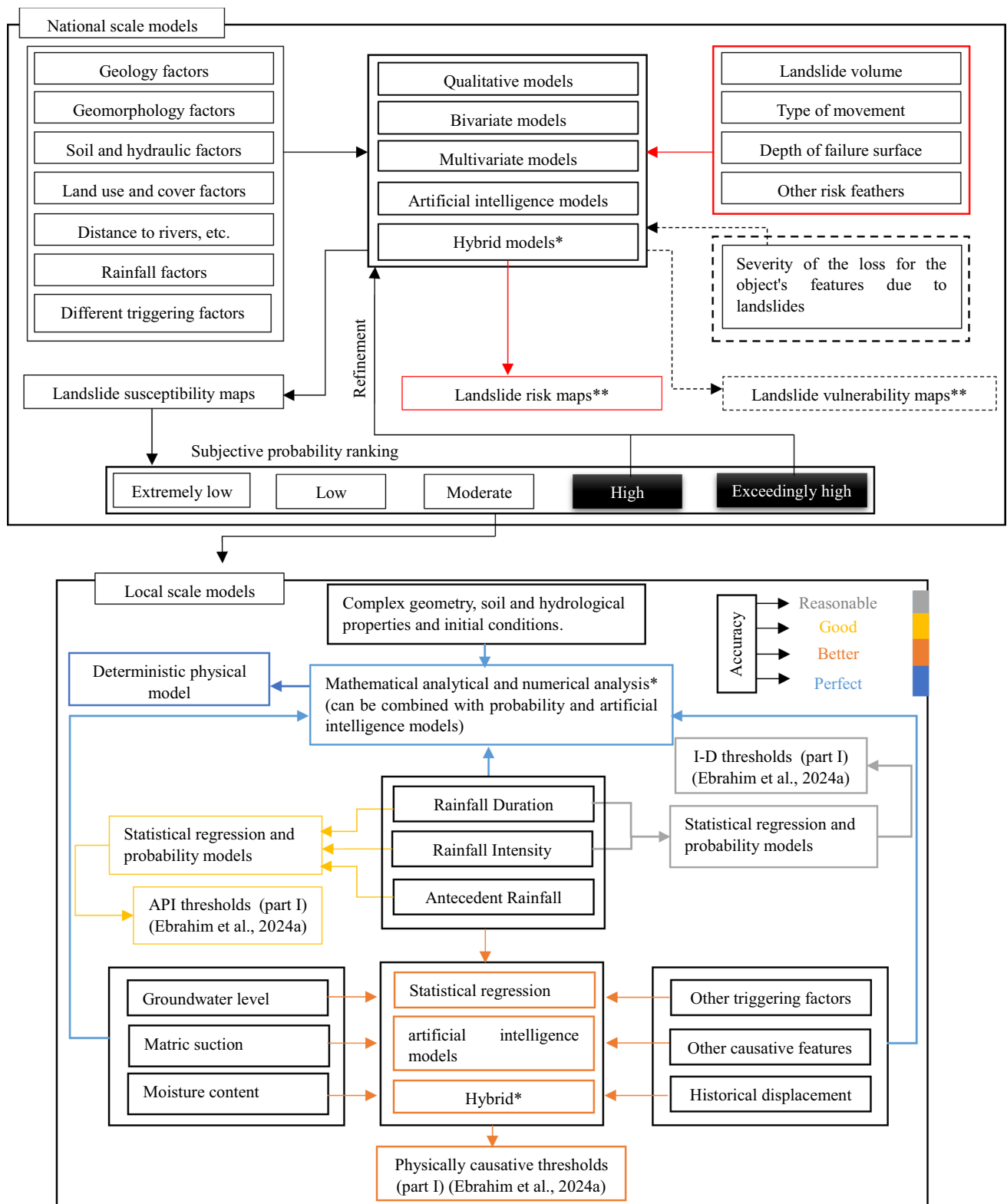


Fig. 18 Different prediction models with their accuracy, input parameters, and analysis techniques. \* Best accuracy, \*\* Out of scope

2006), while for each class, the percentage can differ as shown in Table 2. Hu et al. (2019) and Kainthura and Sharma (2022)

adopted a three-fold classification (low, moderate, and high). Hu et al. (2013), Oh and Lee (2017), Wang and Niu (2010) and

Zhu and Huang (2006) utilized a four-fold classification (very low, low, moderate, and high). Zangmene et al. (2023) employed a four-fold classification (low, moderate, high, and very high). Yang (2017) used a six-fold classification (stable; < 1%; 1 to 5%; 5 to 10%; 10 to 15%; 15 to 20%; 20 to 25%; > 25%).

### Discussion of susceptibility model (advantages, assumptions, and limitations)

Landslide susceptibility maps have an advantage over deterministic studies, as they can be applied to large catchments regardless of the availability of proper detailed geotechnical parameters (Hua et al. 2021). Prediction maps provide an effective, affordable, and quick tool for planners to channel their efforts and resources in areas with higher susceptibility (Liao and Dennis 2004). These maps can aid in decision-making to take appropriate actions to prevent such catastrophes (Karim et al. 2019). For example, landslide susceptibility maps can be used to evaluate the probability of road closure (Yang et al. 2012; Yang 2016), which will help in road maintenance selection and hazard mitigation. In other words, the construction of infrastructure or planning development should be avoided in areas with significant landslide risk unless appropriate landslide mitigation measures are taken (Shano et al. 2021). Landslide susceptibility maps are built based on the assumption that the relationship between the landslide and the feature factor controlling this phenomenon will remain relatively the same in the future (Dang et al. 2019; Wubalem et al. 2022).

Yet, these techniques fail to quantify slope safety over time; all they can do is give the likelihood of landslides or non-landslides. Furthermore, there are certain limits to these models. The performance of the models depends on a number of factors, including the frequency of observations, the ratio of training to testing samples, and the availability of previous landslide data (Hua et al. 2021; Xiao and Zhang 2023; Wubalem et al. 2022). Thus, a sensitivity analysis is required to select the optimal model performance. Therefore, to overcome these drawbacks of the dependency on the volume and accuracy of the dataset (Yao et al. 2014), it is recommended to provide real-time, multi-field (displacement, seepage, stress, etc.) and online observation with high-precision data to establish a real-time extensive dataset (Wang et al. 2023).

### Research gaps and future directions

There are two main ways to improve prediction accuracy. The first is to increase the quality of the input data, while the second is to use new models to achieve greater accuracy. Regarding the dataset itself, it is worth noting that real rainfall patterns and underlying geotechnical properties require improvement. Despite the advances in numerical modelling, several gaps still need to be

filled (refer to Table 5). Dynamic spatiotemporal maps have lately been employed in newly established national regions, although additional research is required (refer to Table 5).

### Conclusions

This study showcased the latest advancements and cutting-edge models for predicting landslides caused by rainfall. These models include physical deterministic models and mapping of landslide susceptibility. Physical models, such as analytical and numerical models, have the capability to attain outstanding precision. These models consider the actual initial conditions, such as slope dimensions, infiltration process, and soil characteristics. Analytical models integrate infiltration analysis (infiltration, evaporation, and surface runoff) with slope stability analysis, considering both saturated and unsaturated conditions. Analytical models can incorporate complex features such as steady-state and transient water flow conditions, the impact of vegetation cover, weathering, degradation, and the neighbouring effect between stable and unstable grids. Recently, the TAG-FLOW model has proven to be the most accurate. Numerical analysis offers various advantages since it uses actual conditions without making any assumptions. Numerical models can simulate various triggering factors in actual conditions (i.e., real rainfall patterns with time delay effects) and create complex 3D geometries. The real bedrock and overlying soil can be simulated precisely considering the hydro-fluctuation effect. Recently, the combination of physical models and probabilistic analysis has been employed to generate susceptibility maps. In addition, physical models may be combined with artificial intelligence models to create an early warning prediction model. However, physical models require thorough geotechnical analysis, which might be unavailable and excessively costly. The aforementioned models are generally suitable for local-scale landslides if spatial input data are available.

Landslide susceptibility maps can be used for land use planning and development. Statistical models used to evaluate such maps are classified as direct (qualitative) or indirect (quantitative). The qualitative approach is based on expert knowledge, whereas quantitative models use various statistical methods to weigh the link between input characteristics. Bivariate models, multivariate models, and artificial intelligence models are included in the quantitative analysis. Bivariate and multivariate models are linear, which makes it difficult to cope with the intricate interaction between triggering factors and slope-controlling characteristics. Artificial intelligence models have recently become popular. These models might be single or hybrid; among all models, hybrid models are believed to give a feasible solution to cope with complicated relationships between controlling characteristics. However, model performance is affected

by both the input parameters and the model used. Dynamic and spatiotemporal susceptibility have recently emerged as prominent study issues.

Despite advancements in deterministic and susceptibility models, several gaps still need to be discovered (see Table 5 for additional information). As a result, an extensive constitutive model that can simulate the weathering process (i.e., rainfall randomness) is suggested to be developed (Postill et al. 2021). Real-time multi-field subsurface monitoring is required to train AI models to forecast such complicated mechanisms. Considering several AI models, different sampling ratios, and data rates helps in selecting the best model and best data set that may help achieve higher prediction accuracy. Groundwater chemistry must be assessed since it may alter the temporal forecast of landslides. Considering dynamic changes in causative features may assist in understanding landslide susceptibility and preventing incorrect predictions. To avoid the subjectivity of susceptibility maps, analyze the physical mechanism of the slope.

In summary, the research is vital as it investigates the procedure for choosing the best model and identifies its essential characteristics. Researchers and professionals seeking innovative methods to decrease the severity of landslides will benefit significantly from the information this study offers. Figure 18 shows models at the local and national scales, input parameters, and accuracy. It examines how one approach leads to another from a macroscopic perspective, depending on input parameters and initial conditions, to a microscopic illustration of different analysis models for the same method.

## Notations

$R_a$ : Antecedent rainfall;  $R_o$ : Rolling rainfall;  $R$ : Cumulative rainfall;  $t$ : Time;  $C$ : Cohesion;  $C'$ : Effective cohesion;  $C(\psi)$ : Moisture capacity;  $\phi$ : Internal friction angle;  $\phi'$ : Effective internal friction angle;  $\phi^b$ : Internal friction angle corresponding to  $\psi$ ;  $\phi'_r$ : Residual friction angle;  $\psi$ : Matrix suction;  $z_{\psi}$ : Matrix suction head;  $v$ : Infiltration velocity;  $u_a$ : Atmospheric pressure;  $u_w$ : Pour water pressure;  $h_w$ : Water head;  $h_b$ : Bubbling pressure;  $I_g$ : Gradient;  $\lambda$ : Pore size index distribution;  $\theta_w$ : Volumetric water content;  $k$ : Unsaturated hydraulic conductivity;  $k_{sat}$ : Saturated hydraulic conductivity;  $k_r$ : Residual hydraulic conductivity;  $q$ : Surface flux;  $Q$ : Discharge;  $\sigma$ : Normal stress;  $\sigma_s$ : Suction stress;  $\tau$ : Shear stress;  $\tau_f$ : Shear strength;  $n_v$ : Viscosity variation with excess shear stress;  $g$ : Gravitational acceleration;  $\gamma_d$ : Dry soil unit weight;  $\gamma_w$ : The unit weight of water;  $\gamma_r$ : Wet unit weight;  $\gamma_{sat}$ : Saturated unit weight;  $G_s$ : Specific gravity;  $n$ : Porosity;  $S_r$ : Degree of saturation;  $S_e$ : Effective saturation;  $T$ : Saturated soil transmissivity;  $W_i$ : Weight of soil;  $H$ : Thickness above the bedrock layer;  $z$ : Unsaturated thickness;  $h$ : Saturated thickness;  $W$ : Width;  $\beta$ : Slope angle;  $m_{sat}$ : Dimensionless thickness for saturated layer;  $T_r$ : Root

failure strength;  $A_r/A$ : Root area ratio;  $f$ : Coefficient function of (friction angle and roots orientation);  $P_f$ : Probability of failure;  $P_r(a)$ : Relative observed agreement;  $P_r(e)$ : Hypothetical probability of chance agreement;  $FS$ : Factor of safety

## Abbreviation

*DBA*: Displacement back analysis; *SWCC*: Soil Water Characteristic Curve; *HCF*: Hydraulic Conductivity Function; *MVG*: Mualem-van Genuchten; *ATI*: Average topographic index; *FRC*: Flow recession coefficient; *TWI*: Topographic witness Index; *NDVI*: Normalized difference vegetation index; *LUC*: Land-use change; *BMFC*: Band math factor combination; *LUFC*: Land-use factor combination; *LUCFC*: Land-use change factor combination; *GA*: Green ampt model; *TOPMODEL*: TOPography-based hydrological MODEL; *SLIDE*: Slope-Infiltration-Distributed Equilibrium; *CREST*: Coupled Routing and Excess Storage; *SLIDE*: Slope-Infiltration-Distributed Equilibrium; *TRIGRS*: Transient Rainfall Infiltration and Grid-based Slope stability; *HIRESSES*: High-Resolution Slope Stability Simulator; *SLIP*: Shallow Landslides Instability Prediction; *LURR*: Loading-Unloading-Response Ratio; *IF*: Indicator function; *3DPLS*: 3-Dimensional Probabilistic Landslide Susceptibility; *MC*: Monte Carlo simulation; *PDF*: Probability density function; *MoSLaPS*: Model Switch-based Landslide Prediction System; *PC4City*: Civil protection for the city; *AUC*: The area under the ROC curve; *ROC*: Receiver operating characteristic; *FPR*: False positive rate;  $R^2$ : Coefficient of determination; *RMSE*: Root mean square error; *MSE*: Mean square error; *MAE*: Mean absolute error; *SDR*: Standard deviation ratio; *PRC*: Pearson-R correlation; *ACC*: Classification Accuracy Rate-CAR; *PPV*: Positive Predictive Value; *NPP*: Negative Predictive Value; *OA*: Overall accuracy; *MCC*: Matthew's correlation coefficient;  $k$ : Kappa index; *AHP*: Analytic hierarchy process; *WLC*: Weighted linear combination; *RVM*: Relevance vector machines; *GLM*: Generalized linear model; *IV*: Information value; *FL*: Fuzzy logic; *TFNW*: Trapezoidal fuzzy number weighting; *FR*: Frequency ratio; *WoE*: Weight of evidence; *CF*: Certainty factor; *IOE*: Index of entropy; *LR*: Logistic regression; *DA*: Discriminate analysis; *ANN*: Artificial neural networks; *MLP*: Multilayer perceptron; *DT*: Decision tree; *BPNN*: Backpropagation neural networks; *SVM*: Support vector mechanism; *RF*: Random forest model; *LSSVM*: Least squares support vector machines; *LSTM*: Long short-term memory; *GRU*: Gated recurrent unite; *DNN*: Deep neural networks; *BT*: Boosted Tree; *BN*: Bayesian networks; *CNN*: Conventional neural network; *AT*: Adaboost tree; *AE*: Autoencoder; *AXBoost*: EXtreme gradient boosting; *GBM*: Generalized boosing machine; *LMT*: Logistic model tree; *LM*: Levenberg–Marquardt algorithm; *BFG*: Broyden Fletcher Goldfarb; *Rp*: Resilient backpropagation; *SCG*: Conjugate gradient with Beale;

*CFG*: Conjugate gradient with Fletcher Reeves' updates; *CGP*: Conjugate Gradient with Polakribiere updates; *OSS*: One Step Secant; *GD*: Gradient Descent; *GDX*: Gradient descent with momentum and adaptive learning rate; *PCA*: Principal component analysis; *GDM*: Gradient Descent with Momentum; *CFNN*: Cascade Forward Neural Network; *ABC*: Artificial bee colony; *SOM*: Self-organizing mapping; *Bi*: Bidirectional; *KNN*: K-Nearest Neighbor; *LASSO*: Least absolute shrinkage and selection operator; *ABT*: Adaboost tree; *DRF*: Distributed random forest; *SFO*: SailFish optimizer; *COA*: Cuckoo optimization algorithm

**Acknowledgements** The authors gratefully acknowledge the fund provided by the Hong Kong Polytechnic University and partially acknowledge the Innovation and Technology Support Programme (ITSP) of the Hong Kong SAR [Grant No. ITS/033/20FP].

**Funding** Open access funding provided by The Hong Kong Polytechnic University.

**Data Availability** The data used in this article were either provided in tables for examples, or are the data that can be found in the cited references.

**Open Access** This article is licensed under a Creative Commons Attribution 4.0 International License, which permits use, sharing, adaptation, distribution and reproduction in any medium or format, as long as you give appropriate credit to the original author(s) and the source, provide a link to the Creative Commons licence, and indicate if changes were made. The images or other third party material in this article are included in the article's Creative Commons licence, unless indicated otherwise in a credit line to the material. If material is not included in the article's Creative Commons licence and your intended use is not permitted by statutory regulation or exceeds the permitted use, you will need to obtain permission directly from the copyright holder. To view a copy of this licence, visit <http://creativecommons.org/licenses/by/4.0/>.

## References

- Abolmasov B, Milenković S, Marjanović M, Đurić U, Jelisavac B (2015) A geotechnical model of the Umka landslide with reference to landslides in weathered Neogene marls in Serbia. *Landslides* 12(4):689–702. <https://doi.org/10.1007/s10346-014-0499-4>
- Al-Batah MS, Alkhasawneh MS, Tay LT, Ngah UK, Lateh H, Mat Isa NA (2015) Landslide occurrence prediction using trainable cascade forward network and multilayer perceptron. *Math Probl Eng* 2015:512158. <https://doi.org/10.1155/2015/512158>
- An H, Viet TT, Lee G, Kim Y, Kim M, Noh S, Noh J (2016) Development of time-variant landslide-prediction software considering three-dimensional subsurface unsaturated flow. *Environ Model Softw* 85:172–183. <https://doi.org/10.1016/j.envsoft.2016.08.009>
- Anbalagan R, Kumar R, Lakshmanan K, Parida S, Neethu S (2015) Landslide hazard zonation mapping using frequency ratio and fuzzy logic approach, a case study of Lachung Valley Sikkim. *Geoenviron Disasters* 2(1):6. <https://doi.org/10.1186/s40677-014-0009-y>

- Arinze EE, Okonkwo UN, Afolabi SO, Ahaiwe CM, Ojobo MO (2021) Geotechnical and Geological Analysis of Amuzukwu Landslide. *Am J Environ Protect* 10(4):84–89. <https://doi.org/10.11648/j.ajep.20211004.12>
- Ayalew L, Yamagishi H (2005) The application of GIS-based logistic regression for landslide susceptibility mapping in the Kakuda-Yahiko Mountains Central Japan. *Geomorphology* 65(1–2):15–31. <https://doi.org/10.1016/j.geomorph.2004.06.010>
- Baum RL, Savage WZ, Godt JW (2008) TRIGRS: a Fortran program for transient rainfall infiltration and grid-based regional slope-stability analysis, version 2.0. U.S. Geological Survey Open-File Report 1159
- Bednarczyk Z (2018) Identification of flysch landslide triggers using conventional and 'nearly real-time monitoring methods—An example from the Carpathian Mountains, Poland. *Eng Geol* 244:41–56. <https://doi.org/10.1016/j.enggeo.2018.07.012>
- Bezerra L, Neto ODF, Santos O Jr, Mickovski S (2020) Landslide risk mapping in an urban area of the city of Natal. Brazil Sustainability (switzerland) 12(22):9601. <https://doi.org/10.3390/su12229601>
- Beven KJ, Kirkby MJ (1979) A physically based, variable contributing area model of basin hydrology/Un modèle à base physique de zone d'appel variable de l'hydrologie du bassin versant. *Hydrol Sci Bull* 24(1):43–69. <https://doi.org/10.1080/02626667909491834>
- Bhardwaj V, Singh K (2023) Landslide Susceptibility Assessment using Remote Sensing and GIS-a. *Journal of Mining and Environment* 14(1):133–154. <https://doi.org/10.22044/jme.2023.12580.2283>
- Biococchi G, Tofani V, D'Ambrosio M, Tacconi-Stefanelli C, Vannocci P, Casagli N, Lavorini G, Trevisani M, Catani F (2019) Geotechnical and hydrological characterization of hillslope deposits for regional landslide prediction modeling. *Bull Eng Geol Env* 78(7):4875–4891. <https://doi.org/10.1007/s10064-018-01449-z>
- Birkinshaw SJ, Ewen J (2000) Nitrogen transformation component for SHETRAN catchment nitrate transport modelling. *J Hydrol* 230(1–2):1–17. [https://doi.org/10.1016/S0022-1694\(00\)00174-8](https://doi.org/10.1016/S0022-1694(00)00174-8)
- Bishop AW (1955) The use of the slip circle in the stability analysis of slopes. *Géotechnique* 5(1):7–17. <https://doi.org/10.1680/geot.1955.5.1.7>
- Calvello M, Cascini L, Grimaldi GM (2009) Displacement scenarios of a rainfall-controlled slow moving active slide in stiff clays. *Georisk* 3(3):116–125. <https://doi.org/10.1080/17499510902793850>
- Cao Y, Yin K, Zhou C, Ahmed B (2020) Establishment of landslide groundwater level prediction model based on GA-SVM and influencing factor analysis. *Sensors (switzerland)* 20(3):845. <https://doi.org/10.3390/s20030845>
- Caine N (1980) The rainfall intensity-duration control of shallow landslides and debris flows. *Geogr Ann Ser B* 62(1–2):23–27. <https://doi.org/10.1080/04353676.1980.11879996>
- Chicco D, Tötsch N, Jurman G (2021) The Matthews correlation coefficient (MCC) is more reliable than balanced accuracy, bookmaker informedness, and markedness in two-class confusion matrix evaluation. *BioData Mining* 14(1):13. <https://doi.org/10.1186/s13040-021-00244-z>
- Cho SE (2017) Prediction of shallow landslide by surficial stability analysis considering rainfall infiltration. *Eng Geol* 231:126–138. <https://doi.org/10.1016/j.enggeo.2017.10.018>
- Chae BG, Park HJ, Catani F, Simoni A, Berti M (2017) Landslide prediction, monitoring and early warning: a concise review of state-of-the-art. *Geosci J* 21(6):1033–1070. <https://doi.org/10.1007/s12303-017-0034-4>
- Chae BG, Wu YH, Liu KF, Choi J, Park HJ (2020) Simulation of debris-flow runout near a construction site in Korea. *Appl Sci* 10(17):6079. <https://doi.org/10.3390/app10176079>

- Chen ZY, Morgenstern N (1983) Extensions to the generalized method of slices for stability analysis. *Can Geotech J* 20(1):104–119. <https://doi.org/10.1139/t83-010>
- Chen X, Zhang L, Chen L, Li X, Liu D (2019) Slope stability analysis based on the Coupled Eulerian-Lagrangian finite element method. *Bull Eng Geol Env* 78(6):4451–4463. <https://doi.org/10.1007/s10064-018-1413-4>
- Collini E, Palesi LI, Nesi P, Pantaleo G, Nocentini N, Rosi A (2022) Predicting and understanding landslide events with explainable AI. *IEEE Access* 10:31175–31189. <https://doi.org/10.1109/ACCESS.2022.3158328>
- Collins BD, Znidarcic D (2004) Stability analyses of rainfall induced landslides. *J Geotech Geoenviron Eng* 130(4):362–372. [https://doi.org/10.1061/\(ASCE\)1090-0241\(2004\)130:4\(362\)](https://doi.org/10.1061/(ASCE)1090-0241(2004)130:4(362))
- Corominas J, Guzzetti F, Lan H, Macciotta R, Marunteranu C, McDougall S, Strom A (2023) Revisiting landslide risk terms: IAEG commission C-37 working group on landslide risk nomenclature. *Bull Eng Geol Env* 82(12):450. <https://doi.org/10.1007/s10064-023-03474-z>
- Cuomo S, Di Perna A, Martinelli M (2021) Modelling the spatio-temporal evolution of a rainfall-induced retrogressive landslide in an unsaturated slope. *Eng Geol* 294:106371. <https://doi.org/10.1016/j.enggeo.2021.106371>
- Dai Y, Dai W, Yu W, Bai D (2022) Determination of landslide displacement warning thresholds by applying DBA-LSTM and numerical simulation algorithms. *Appl Sci (switzerland)* 12(13):6690. <https://doi.org/10.3390/app12136690>
- Dang VH, Dieu TB, Tran XL, Hoang ND (2019) Enhancing the accuracy of rainfall-induced landslide prediction along mountain roads with a GIS-based random forest classifier. *Bull Eng Geol Env* 78(4):2835–2849. <https://doi.org/10.1007/s10064-018-1273-y>
- Das P, Patwa D, Bharat TV (2022) Influencing factors on the simulation of rainfall-induced landslide prediction based on case study. *Bull Eng Geol Env* 81(5):194. <https://doi.org/10.1007/s10064-022-02682-3>
- Davar S, Nobahar M, Khan MS, Amini F (2022) The development of PSO-ANN and BOA-ANN models for predicting matric suction in expansive clay soil. *Mathematics* 10(16):2825. <https://doi.org/10.3390/math10162825>
- Depina I, Oguz EA, Thakur V (2020) Novel Bayesian framework for calibration of spatially distributed physical-based landslide prediction models. *Comput Geotech* 125:103660. <https://doi.org/10.1016/j.compgeo.2020.103660>
- De Graff JV (2011) Perspectives for systematic landslide monitoring. *Environ Eng Geosci* 17(1):67–76. <https://doi.org/10.2113/gseeg.17.1.67>
- Duncan JM (1996) State of the art: limit equilibrium and finite-element analysis of slopes. *J Geotechn Eng* 122(7):577–596. [https://doi.org/10.1061/\(ASCE\)0733-9410\(1996\)122:7\(577\)](https://doi.org/10.1061/(ASCE)0733-9410(1996)122:7(577))
- Ebrahim KMP, Gomaa SMMH, Zayed T, Alfalah G (2024a) Landslide prediction models, Part I: Empirical-statistical and physically based causative thresholds [Manuscript submitted for publication]. Faculty of Construction and Environment, The Hong Kong Polytechnic University, Department of Building and Real Estate
- Ebrahim KMP, Gomaa SMMH, Zayed T, Alfalah G (2024b) Phenomenal and investigational recent subsurface landslide monitoring techniques: A mixed review. *Remote Sensing* 16(2):385. <https://doi.org/10.3390/rs16020385>
- Fawcett T (2006) An introduction to ROC analysis. *Pattern Recogn Lett* 27(8):861–874. <https://doi.org/10.1016/j.patrec.2005.10.010>
- Fell R, Corominas J, Bonnard C, Cascini L, Leroi E, Savage WZ (2008) Guidelines for landslide susceptibility, hazard and risk zoning for land use planning. *Eng Geol* 102(3):85–98. <https://doi.org/10.1016/j.enggeo.2008.03.022>
- Feng Y, Yan F, Wu L, Lu G, Liu T (2023) Numerical Analyses of Slope Stability Considering Grading and Seepage Prevention. *Water* 15(9):1745. <https://www.mdpi.com/2073-4441/15/9/1745>
- Formetta G, Capparelli G (2019) Quantifying the three-dimensional effects of anisotropic soil horizons on hillslope hydrology and stability. *J Hydrol* 570:329–342. <https://doi.org/10.1016/j.jhydrol.2018.12.064>
- Fredlund DG, Rahardjo H (1993) Soil mechanics for unsaturated soils. John Wiley and Sons
- Fredlund DG, Krahn J (1977) Comparison of slope stability methods of analysis. *Can Geotech J* 14(3):429–439. <https://doi.org/10.1139/t77-045>
- Gerscovich DMS, Vargas EA Jr, De Campos TMP (2006) On the evaluation of unsaturated flow in a natural slope in Rio de Janeiro. *Brazil Eng Geol* 88(1–2):23–40. <https://doi.org/10.1016/j.enggeo.2006.07.008>
- Guo C, Wu J, Zhao S, Wang Z, Meena SR, Zhang F (2022) Landslide susceptibility assessment based on multi GPUs: A deep learning approach. *CCF Trans High Performance Comput* 4(2):135–149. <https://doi.org/10.1007/s42514-022-00097-w>
- Green WH, Ampt GA (1911) Studies on Soil Physics. *J Agric Sci* 4(1):1–24. <https://doi.org/10.1017/S0021859600001441>
- Giri P, Ng K, Phillips W (2018) Wireless sensor network system for landslide monitoring and warning. *IEEE Trans Instrum Meas* 68(4):1210–1220. <https://doi.org/10.1109/TIM.2018.2861999>
- Hanafiah MIM, Solemon B, Omar R, Roslan R, Wahab WA, Bahardin INZ, Gunasagaran V (2019) Landslide susceptibility assessment for cameron highlands using analytical hierarchy process. *Int J Eng Adv Technol* 9(1):3494–3499. <https://doi.org/10.35940/ijeat.A2673.109119>
- Harsa H, Hidayat AM, Mulsandi A, Suprihadi B, Kurniawan R, Habibie MN, Hutapea TD, Swarinoto YS, Makmur EES, Fitriah W, Sri Sudewi RS, Praja AS (2023) Machine learning and artificial intelligence models development in rainfall-induced landslide prediction. *IAES Int J Artif Intell* 12(1):262–270. <https://doi.org/10.11591/ijai.v12.i1.pp262-270>
- He J, Wang S, Liu H, Nguyen V, Han W (2021) The critical curve for shallow saturated zone in soil slope under rainfall and its prediction for landslide characteristics. *Bull Eng Geol Env* 80(3):1927–1945. <https://doi.org/10.1007/s10064-020-02016-1>
- He X, Hong Y, Vergara H, Zhang K, Kirstetter PE, Gourley JJ, Zhang Y, Qiao G, Liu C (2016) Development of a coupled hydrological-geotechnical framework for rainfall-induced landslides prediction. *J Hydrol* 543(Part B):395–405. <https://doi.org/10.1016/j.jhydrol.2016.10.016>
- Ho JY, Lee KT (2017) Performance evaluation of a physically based model for shallow landslide prediction. *Landslides* 14(3):961–980. <https://doi.org/10.1007/s10346-016-0762-y>
- Ho JY, Lee KT, Chang TC, Wang ZY, Liao YH (2012) Influences of spatial distribution of soil thickness on shallow landslide prediction. *Eng Geol* 124(1):38–46. <https://doi.org/10.1016/j.enggeo.2011.09.013>
- Hobbs PRN, Jones LD, Kirkham MP, Pennington CVL, Morgan DJR, Dashwood C (2020) Coastal landslide monitoring at aldbrough, east riding of Yorkshire, UK. *Q J Eng GeolHydrogeol* 53(1):101–116. <https://doi.org/10.1144/qjgeh2018-210>
- Hong M, Kim J, Jeong S (2018) Rainfall intensity-duration thresholds for landslide prediction in South Korea by considering the effects of antecedent rainfall. *Landslides* 15(3):523–534. <https://doi.org/10.1007/s10346-017-0892-x>
- Hu J, Zhu H, Mao Y, Zhang C, Liang T, Mao D (2019) Using uncertain DM-chameleon clustering algorithm based on machine learning to predict landslide hazards. *J Robotics Mechatron* 31(2):329–338. <https://doi.org/10.20965/jrm.2019.p0329>

- Hu Z, Wei L, Fang D, Lai T, Wang Q (2013) Spatial prediction of earthquake-induced secondary landslide disaster in Beichuan County based on GIS. *Res J Appl Sci Eng Technol* 6(20):3828–3837. <https://doi.org/10.19026/rjaset.6.3598>
- Hua Y, Wang X, Li Y, Xu P, Xia W (2021) Dynamic development of landslide susceptibility based on slope unit and deep neural networks. *Landslides* 18(1):281–302. <https://doi.org/10.1007/s10346-020-01444-0>
- Huang J, Ju NP, Liao YJ, Liu DD (2015) Determination of rainfall thresholds for shallow landslides by a probabilistic and empirical method. *Nat Hazard* 15(12):2715–2723. <https://doi.org/10.5194/nhess-15-2715-2015>
- Huang J, Wu X, Ling S, Li X, Wu Y, Peng L, He Z (2022) A bibliometric and content analysis of research trends on GIS-based landslide susceptibility from 2001 to 2020. *Environ Sci Pollut Res* 29(58):86954–86993. <https://doi.org/10.1007/s11356-022-23732-z>
- Huang Y, He Z (2023) Rainfall-oriented resilient design for slope system: Resilience-enhancing strategies. *Soils Found* 63(2):101297. <https://doi.org/10.1016/j.sandf.2023.101297>
- Huo YX, Gomaa SM, Zayed T, Meguid M (2023) Review of analytical methods for stress and deformation analysis of buried water pipes considering pipe-soil interaction. *Underground Space* 13:205–227. <https://doi.org/10.1016/j.undsp.2023.02.017>
- Hwang IT, Park HJ, Lee JH (2023) Probabilistic analysis of rainfall-induced shallow landslide susceptibility using a physically based model and the bootstrap method. *Landslides* 20(4):829–844. <https://doi.org/10.1007/s10346-022-02014-2>
- Ikram RMA, Dehrashid AA, Zhang B, Chen Z, Le BN, Moayedi H (2023) A novel swarm intelligence: cuckoo optimization algorithm (COA) and SailFish optimizer (SFO) in landslide susceptibility assessment. *Stoch Env Res Risk Assess* 37(5):1717–1743. <https://doi.org/10.1007/s00477-022-02361-5>
- Ji J, Cui H, Zhang T, Song J, Gao Y (2022) A GIS-based tool for probabilistic physical modelling and prediction of landslides: GIS-FORM landslide susceptibility analysis in seismic areas. *Landslides* 19(9):2213–2231. <https://doi.org/10.1007/s10346-022-01885-9>
- Kainthura P, Sharma N (2022) Machine learning driven landslide susceptibility prediction for the Uttarkashi region of Uttarakhand in India. *Georisk: Assess Manag Risk for Eng Syst Geohazards* 16(3):570–583. <https://doi.org/10.1080/17499518.2021.1957484>
- Karim Z, Hadji R, Hamed Y (2019) GIS-based approaches for the landslide susceptibility prediction in Setif Region (NE Algeria). *Geotech Geol Eng* 37(1):359–374. <https://doi.org/10.1007/s10706-018-0615-7>
- Khan MI, Wang S (2021) Slope stability analysis to correlate shear strength with slope angle and shear stress by considering saturated and unsaturated seismic conditions. *Appl Sci (switzerland)* 11(10):4568. <https://doi.org/10.3390/app11104568>
- Lee KT, Ho JY (2009) Prediction of landslide occurrence based on slope-instability analysis and hydrological model simulation. *J Hydrol* 375(3–4):489–497. <https://doi.org/10.1016/j.jhydrol.2009.06.053>
- Lee W-L, Martinelli M, Shieh C-L (2021) An Investigation of Rainfall-Induced Landslides From the Pre-Failure Stage to the Post-Failure Stage Using the Material Point Method. *Front Earth Sci* 9:764393. <https://doi.org/10.3389/feart.2021.764393>
- Li Y, Utili S, Milledge D, Chen L, Yin K (2021) Chasing a complete understanding of the failure mechanisms and potential hazards of the slow moving Liangshuijing landslide. *Eng Geol* 281:105977. <https://doi.org/10.1016/j.enggeo.2020.105977>
- Liang WL, Uchida T (2022) Performance and topographic preferences of dynamic and steady models for shallow landslide prediction in a small catchment. *Landslides* 19(1):51–66. <https://doi.org/10.1007/s10346-021-01771-w>
- Liao Q, Dennis ND (2004) Focusing landslide investigation efforts with geographic information system screening techniques. *Transp Res Rec* 1868(1):113–123. <https://doi.org/10.3141/1868-12>
- Liao Z, Hong Y, Wang J, Fukuoka H, Sassa K, Karnawati D, Fathani F (2010) Prototyping an experimental early warning system for rainfall-induced landslides in Indonesia using satellite remote sensing and geospatial datasets. *Landslides* 7(3):317–324. <https://doi.org/10.1007/s10346-010-0219-7>
- Liu X, Wang Y, Koo RC, Kwan JS (2022) Development of a slope digital twin for predicting temporal variation of rainfall-induced slope instability using past slope performance records and monitoring data. *Eng Geol* 308:106825. <https://doi.org/10.1016/j.enggeo.2022.106825>
- Liu X, Wang Y, Li D-Q (2020) Numerical simulation of the 1995 rainfall-induced Fei Tsui Road landslide in Hong Kong: new insights from hydro-mechanically coupled material point method. *Landslides* 17:2755–2775. <https://doi.org/10.1007/s10346-020-01442-2>
- Long J, Liu Y, Li C, Fu Z, Zhang H (2021) A novel model for regional susceptibility mapping of rainfall-reservoir induced landslides in Jurassic slide-prone strata of western Hubei Province, Three Gorges Reservoir area. *Stoch Env Res Risk Assess* 35(7):1403–1426. <https://doi.org/10.1007/s00477-020-01892-z>
- Manchar N, Benabbas C, Hadji R, Bouaicha F, Grecu F (2018) Landslide susceptibility assessment in Constantine region (NE Algeria) by means of statistical models. *Studia Geotechnica Et Mechanica* 40(3):208–219. <https://doi.org/10.2478/sgem-2018-0024>
- Marrapu BM, Kukunuri A, Jakka RS (2021) Improvement in prediction of slope stability & relative importance factors using ANN. *Geotech Geol Eng* 39(8):5879–5894. <https://doi.org/10.1007/s10706-021-01872-2>
- Ma J, Tang H, Hu X, Bobet A, Yong R, Ez Eldin MA (2017) Model testing of the spatial-temporal evolution of a landslide failure. *Bull Eng Geol Env* 76(1):323–339. <https://doi.org/10.1007/s10064-016-0884-4>
- Matyas EL, Radhakrishna HS (1968) Volume Change Characteristics of Partially Saturated Soils. *Géotechnique* 18(4):432–448. <https://doi.org/10.1680/geot.1968.18.4.432>
- Medwedeff WG, Clark MK, Zekkos D, West AJ (2020) Characteristic landslide distributions: An investigation of landscape controls on landslide size. *Earth Planet Sci Lett* 539:116203. <https://doi.org/10.1016/j.epsl.2020.116203>
- Merghadi A, Yunus AP, Dou J, Whiteley J, ThaiPham B, Bui DT, Avtar R, Abderrahmane B (2020) Machine learning methods for landslide susceptibility studies: A comparative overview of algorithm performance. *Earth Sci Rev* 207:103225. <https://doi.org/10.1016/j.earscirev.2020.103225>
- Midhuna V, Grurugnanam B, Bairavi S (2022) Landslide Susceptibility Mapping using Frequency Ratio, a case study of Vythiriblock in Wayanad, the northern part of Kerala India. *Disaster Adv* 15(1):1–15. <https://doi.org/10.25303/1501da001015>
- Mondini AC, Guzzetti F, Melillo M (2023) Deep learning forecast of rainfall-induced shallow landslides. *Nat Commun* 14(1):2466. <https://doi.org/10.1038/s41467-023-38135-y>
- Morgenstern NU, Price VE (1965) The analysis of the stability of general slip surfaces. *Géotechnique* 15(1):79–93. <https://doi.org/10.1680/geot.1965.15.1.79>
- Ng CWW, Yang B, Liu ZQ, Kwan JSH, Chen L (2021) Spatiotemporal modelling of rainfall-induced landslides using machine learning. *Landslides* 18(7):2499–2514. <https://doi.org/10.1007/s10346-021-01662-0>
- Nguyen TS, Likitlersuang S, Jotisankasa A (2019) Influence of the spatial variability of the root cohesion on a slope-scale stability model: a case study of residual soil slope in Thailand.

- Bull Eng Geol Env 78(5):3337–3351. <https://doi.org/10.1007/s10064-018-1380-9>
- Oguz EA, Depina I, Thakur V (2022) Effects of soil heterogeneity on susceptibility of shallow landslides. *Landslides* 19(1):67–83. <https://doi.org/10.1007/s10346-021-01738-x>
- Oh HJ, Lee S (2017) Shallow landslide susceptibility modeling using the data mining models artificial neural network and boosted tree. *Applied Sciences (switzerland)* 7(10):1000. <https://doi.org/10.3390/app7101000>
- Oliveira EdP, Acevedo AMG, Moreira VS, Faro VP, Kormann ACM (2022) The Key Parameters Involved in a Rainfall-Triggered Landslide. *Water* 14(21): 3561. <https://www.mdpi.com/2073-4441/14/21/3561>
- Pagano L, Picarelli L, Rianna G, Urciuoli G (2010) A simple numerical procedure for timely prediction of precipitation-induced landslides in unsaturated pyroclastic soils. *Landslides* 7(3):273–289. <https://doi.org/10.1007/s10346-010-0216-x>
- Pecoraro G, Nicodemo G, Menichini R, Luongo D, Peduto D, Calvello M (2023) Combining Statistical, Displacement and Damage Analyses to Study Slow-Moving Landslides Interacting with Roads: Two Case Studies in Southern Italy. *Appl Sci* 13(5):3368. <https://doi.org/10.3390/app13053368>
- Perrin C, Michel C, Andréassian V (2003) Improvement of a parsimonious model for streamflow simulation. *J Hydrol* 279(1–4):275–289. [https://doi.org/10.1016/S0022-1694\(03\)00225-7](https://doi.org/10.1016/S0022-1694(03)00225-7)
- Petrucci O (2022) Landslide fatality occurrence: a systematic review of research published between January 2010 and March 2022. *Sustainability (switzerland)* 14(15):9346. <https://doi.org/10.3390/su14159346>
- Postill H, Helm PR, Dixon N, Glendinning S, Smethurst JA, Rouainia M, Briggs KM, El-Hamalawi A, Blake AP (2021) Forecasting the long-term deterioration of a cut slope in high-plasticity clay using a numerical model. *Eng Geol* 280:105912. <https://doi.org/10.1016/j.enggeo.2020.105912>
- Purnama AY, Latif DO, Kurniawan AW, Adriyati M (2022) Implementation of building information modeling on slope stability and mitigation analysis in Aceh Indonesia. *J Appl Eng Sci* 20(1):293–299. <https://doi.org/10.5937/jaes0-29558>
- Qiu D, Wang L, Luo D, Huang H, Ye Q, Zhang Y (2019) Landslide monitoring analysis of single-frequency BDS/GPS combined positioning with constraints on deformation characteristics. *Surv Rev* 51(367):364–372. <https://doi.org/10.1080/00396265.2018.1467075>
- Rahimi A, Rahardjo H, Leong EC (2010) Effect of hydraulic properties of soil on rainfall-induced slope failure. *Eng Geol* 114(3–4):135–143. <https://doi.org/10.1016/j.enggeo.2010.04.010>
- Richards LA (1931) Capillary conduction of liquids through porous mediums. *J Appl Phys* 1(5):318–333. <https://doi.org/10.1063/1.1745010>
- Riaz MT, Basharat M, Brunetti MT, Riaz MT (2023) Semi-quantitative landslide risk assessment of district Muzaffarabad, northwestern Himalayas, Pakistan. *Stoch Env Res Risk Assess* 37(9):3551–3570. <https://doi.org/10.1007/s00477-023-02462-9>
- Román-Herrera JC, Rodríguez-Peces MJ, Garzón-Roca J (2023) Comparison between Machine Learning and Physical Models Applied to the Evaluation of Co-Seismic Landslide Hazard. *Appl Sci* 13(14):8285. <https://doi.org/10.3390/app13148285>
- Rossi G, Catani F, Leoni L, Segoni S, Tofani V (2013) HIRESSS: a physically based slope stability simulator for HPC applications. *Nat Hazards Earth Syst Sci* 13(1):151–166. <https://doi.org/10.5194/nhess-13-151-2013>
- Saadatkah N, Kassim A, Lee LM (2015) Hulu Kelang, Malaysia regional mapping of rainfall-induced landslides using TRIGRS model. *Arab J Geosci* 8(5):3183–3194. <https://doi.org/10.1007/s12517-014-1410-2>
- Salciarini D, Fanelli G, Tamagnini C (2017) A probabilistic model for rainfall—induced shallow landslide prediction at the regional scale. *Landslides* 14(5):1731–1746. <https://doi.org/10.1007/s10346-017-0812-0>
- Salvatici T, Tofani V, Rossi G, D’Ambrosio M, Tacconi Stefanelli C, Benedetta Masi E, Rosi A, Pazzi V, Vannocci P, Petrolo M, Catani F, Ratto S (2018) Application of a physically based model to forecast shallow landslides at a regional scale. *Nat Hazard* 18(7):1919–1935. <https://doi.org/10.5194/nhess-18-1919-2018>
- Sarma S (1987) A note on the stability analysis of slopes. *Géotechnique* 37(1):107–111. <https://doi.org/10.1680/geot.1987.37.1.107>
- Segoni S, Piciullo L, Gariano SL (2018) A review of the recent literature on rainfall thresholds for landslide occurrence. *Landslides* 15(8):1483–1501. <https://doi.org/10.1007/s10346-018-0966-4>
- Schaap MG, Van Genuchten MT (2006) A modified Mualem–van Genuchten formulation for improved description of the hydraulic conductivity near saturation. *Vadose Zone Journal* 5(1):27–34. <https://doi.org/10.2136/vzj2005.0005>
- Selamat SN, Abd Majid N, Mohd Taib A (2023) A Comparative Assessment of Sampling Ratios Using Artificial Neural Network (ANN) for Landslide Predictive Model in Langat River Basin, Selangor Malaysia. *Sustainability (switzerland)* 15(1):861. <https://doi.org/10.3390/su15010861>
- Shah NA, Shafique M, Ishfaq M, Faisal K, Van der Meijde M (2023) Integrated Approach for Landslide Risk Assessment Using Geoinformation Tools and Field Data in Hindukush Mountain Ranges, Northern Pakistan. *Sustainability (switzerland)* 15(4):3102. <https://doi.org/10.3390/su15043102>
- Shano L, Raghuvanshi TK, Meten M (2020) Landslide susceptibility evaluation and hazard zonation techniques—a review. *Geoenviron Disasters* 7(1):18. <https://doi.org/10.1186/s40677-020-00152-0>
- Shano L, Raghuvanshi TK, Meten M (2021) Landslide hazard zonation using logistic regression model: The case of Shafe and Baso catchments, Gamo highland Southern Ethiopia. *Geotech Geol Ineering* 40(1):83–101. <https://doi.org/10.1007/s10706-021-01873-1>
- Sharma S, Mahajan AK (2018) Comparative evaluation of GIS-based landslide susceptibility mapping using statistical and heuristic approach for Dharamshala region of Kangra Valley India. *Geoenviron Disasters* 5(1):4. <https://doi.org/10.1186/s40677-018-0097-1>
- Shu HM, Chen TC, Yang WC, Luo YX (2016) Interpretation and Analysis of Potential Fluidized Landslide Slope. *Geotechn Eng J SEAGS and AGSSEA* 47(2):101–111
- Sim J, Wright CC (2005) The kappa statistic in reliability studies: use, interpretation, and sample size requirements. *Phys Ther* 85(3):257–268. <https://doi.org/10.1093/ptj/85.3.257>
- Sitarenios P, Casini F, Askarinejad A, Springman S (2021) Hydro-mechanical analysis of a surficial landslide triggered by artificial rainfall: the Ruedlingen field experiment. *Geotechnique* 71(2):96–109. <https://doi.org/10.1680/jgeot.18.P.188>
- Soga K, Alonso E, Yerro A, Kumar K, Bandara S (2016) Trends in large-deformation analysis of landslide mass movements with particular emphasis on the material point method. *Geotechnique* 66(3):248–273. <https://doi.org/10.1680/jgeot.15.LM.005>
- Song Z, Li X, Lizárraga JJ, Zhao L, Buscarnera G (2020) Spatially distributed landslide triggering analyses accounting for coupled infiltration and volume change. *Landslides* 17(12):2811–2824. <https://doi.org/10.1007/s10346-020-01451-1>
- Spencer E (1967) A method of analysis of the stability of embankments assuming parallel inter-slice forces. *Géotechnique* 17(1):11–26. <https://doi.org/10.1680/geot.1967.17.1.11>
- Stehman SV (1997) Selecting and interpreting measures of thematic classification accuracy. *Remote Sens Environ* 62(1):77–89. [https://doi.org/10.1016/S0034-4257\(97\)00083-7](https://doi.org/10.1016/S0034-4257(97)00083-7)

- Sun J, Yu T, Dong P (2022) Evaluation of 3D slope stability based on the minimum potential energy principle. *Comput Geotech* 146:104717. <https://doi.org/10.1016/j.compgeo.2022.104717>
- Tang Y, Wu W, Yin K, Wang S, Lei G (2019) A hydro-mechanical coupled analysis of rainfall induced landslide using a hypoplastic constitutive model. *Comput Geotech* 112:284–292. <https://doi.org/10.1016/j.compgeo.2019.04.024>
- Tengtrairat N, Woo WL, Parathai P, Aryupong C, Jitsangiam P, Rinchumphu D (2021) Automated landslide-risk prediction using web gis and machine learning models. *Sensors (switzerland)* 21(13):4620. <https://doi.org/10.3390/s21134620>
- Thang NV, Wakai A, Sato G, Viet TT, Kitamura N (2022) Simple Method for Shallow Landslide Prediction Based on Wide-Area Terrain Analysis Incorporated with Surface and Subsurface Flows. *Nat Hazard Rev* 23(4):04022028. [https://doi.org/10.1061/\(ASCE\)NH.1527-6996.0000578](https://doi.org/10.1061/(ASCE)NH.1527-6996.0000578)
- Tien Bui D, Tuan TA, Hoang ND, Thanh NQ, Nguyen DB, Van Liem N, Pradhan B (2017) Spatial prediction of rainfall-induced landslides for the Lao Cai area (Vietnam) using a hybrid intelligent approach of least squares support vector machines inference model and artificial bee colony optimization. *Landslides* 14(2):447–458. <https://doi.org/10.1007/s10346-016-0711-9>
- Uchida T, Mori N, Tamura K, Terada H, Takiguchi S, Kamee K (2009) The role of data preparation on shallow landslide prediction. *J Japan Soc Erosion Control Eng* 62(1):23–31
- Utomo D, Chen SF, Hsiung PA (2019) Landslide prediction with model switching. *Appl Sci (switzerland)* 9(9):1839. <https://doi.org/10.3390/app9091839>
- Valentino R, Meisina C, Montrasio L, Losi GL, Zizioli D (2014) Predictive power evaluation of a physically based model for shallow landslides in the area of Oltrepò Pavese Northern Italy. *Geotechn Geol Eng* 32(4):783–805. <https://doi.org/10.1007/s10706-014-9758-3>
- Varnes DJ (1984) Landslide hazard zonation: a review of principles and practice, United Nations Educational, Scientific and Cultural Organization. *Nat Hazards* 3
- Wan LP, Zhou ML, Desai S (2017) Long-term stability calculation of reservoir bank slope considering water-rock interaction. *Tehnicki vjesnik/Technical Gazette* 24(1):283–289. <https://doi.org/10.17559/TV-20160517083309>
- Wang JJ, Liang Y, Zhang HP, Wu Y, Lin X (2014) A loess landslide induced by excavation and rainfall. *Landslides* 11(1):141–152. <https://doi.org/10.1007/s10346-013-0418-0>
- Wang J, Hong Y, Li L, Gourley JJ, Khan SI, Yilmaz KK, Adler RF, Policelli FS, Habib S, Irwin D, Limaye AS, Korme T (2011) The coupled routing and excess storage (CREST) distributed hydrological model. *Hydrol Sci J* 56(1):84–98. <https://doi.org/10.1080/02626667.2010.543087>
- Wang L, Yan E, Wang Y, Huang S, Liu Y (2016) Load-Unload Response Characteristics and Prediction of Reservoir Landslides. *Electron J Geotech Eng* 21(17):5599–5608
- Wang R, Zhang K, Wang W, Meng Y, Yang L, Huang H (2023) Hydrodynamic landslide displacement prediction using combined extreme learning machine and random search support vector regression model. *Eur J Environ Civ Eng* 27(6):2345–2357. <https://doi.org/10.1080/19648189.2020.1754298>
- Wang S, Zhang K, van Beek LP, Tian X, Bogaard TA (2020) Physically-based landslide prediction over a large region: Scaling low-resolution hydrological model results for high-resolution slope stability assessment. *Environ Model Softw* 124:104607. <https://doi.org/10.1016/j.envsoft.2019.104607>
- Wang WD, Xie CM, Du XG (2009) Landslides susceptibility mapping in Guizhou province based on fuzzy theory. *Mining Sci ogy (china)* 19(3):399–404. [https://doi.org/10.1016/S1674-5264\(09\)60075-2](https://doi.org/10.1016/S1674-5264(09)60075-2)
- Wang X, Niu R (2010) Landslide intelligent prediction using object-oriented method. *Soil Dyn Earthq Eng* 30(12):1478–1486. <https://doi.org/10.1016/j.soildyn.2010.06.017>
- Wu L, Huang R, Li X (2020) Hydro-mechanical analysis of rainfall-induced landslides. Springer Singapore, 1–235. <https://doi.org/10.1007/978-981-15-0761-8>
- Wu YM, Lan HX, Gao X, Li LP, Yang ZH (2015) A simplified physically based coupled rainfall threshold model for triggering landslides. *Eng Geol* 195:63–69. <https://doi.org/10.1016/j.enggeo.2015.05.022>
- Wubalem A (2021) Landslide susceptibility mapping using statistical methods in Uatza catchment area, northwestern Ethiopia. *Geoenviron Disasters* 8(1):1. <https://doi.org/10.1186/s40677-020-00170-y>
- Wubalem A, Meten M (2020) Landslide susceptibility mapping using information value and logistic regression models in Goncha Siso Eneses area, northwestern Ethiopia. *Applied Sciences* 2:1–19. <https://doi.org/10.1007/s42452-020-2563-0>
- Wubalem A, Getahun B, Hailemariam Y, Mesele A, Tesfaw G, Dawit Z, Goshe E (2022) Landslide susceptibility modeling using the index of entropy and frequency ratio method from nefas-mewcha to weldiya road corridor, northwestern Ethiopia. *Geotech Geol Eng* 40(10):5249–5278. <https://doi.org/10.1007/s10706-022-02214-6>
- Xiao T, Zhang LM (2023) Data-driven landslide forecasting: Methods, data completeness, and real-time warning. *Eng Geol* 317:107068. <https://doi.org/10.1016/j.enggeo.2023.107068>
- Xiao T, Zhang LM, Cheung RWM, Lacasse S (2022) Predicting spatio-temporal man-made slope failures induced by rainfall in Hong Kong using machine learning techniques. *Géotechnique* 1–17. <https://doi.org/10.1680/jgeot.21.00160>
- Xu W, Xu H, Chen J, Kang Y, Pu Y, Ye Y, Tong J (2022) Combining numerical simulation and deep learning for landslide displacement prediction: An attempt to expand the deep learning dataset. *Sustainability (switzerland)* 14(11):6908. <https://doi.org/10.3390/su14116908>
- Yang P, Wang N, Guo Y, Ma X, Wang C (2022) Performance Analysis of Logistic Model Tree-Based Ensemble Learning Algorithms for Landslide Susceptibility Mapping. *J Sensors* 2022:8254356. <https://doi.org/10.1155/2022/8254356>
- Yang SR, Shen CW, Huang CM, Lee CT, Cheng CT, Chen CY (2012) Prediction of mountain road closure due to rainfall-induced landslides. *J Perform Constr Facil* 26(2):197–202. [https://doi.org/10.1061/\(ASCE\)CF.1943-5509.0000242](https://doi.org/10.1061/(ASCE)CF.1943-5509.0000242)
- Yang SR (2016) Probability of road interruption due to landslides under different rainfall-return periods using remote sensing techniques. *J Perform Constr Facil* 30(1):C4015002. [https://doi.org/10.1061/\(ASCE\)CF.1943-5509.0000737](https://doi.org/10.1061/(ASCE)CF.1943-5509.0000737)
- Yang SR (2017) Assessment of rainfall-induced landslide susceptibility using GIS-based slope unit approach. *J Perform Constr Facil* 31(4):04017026. [https://doi.org/10.1061/\(ASCE\)CF.1943-5509.0000997](https://doi.org/10.1061/(ASCE)CF.1943-5509.0000997)
- Yang X, Diao X, Zhou T, Hu F, Wang S (2023) Study on the stability of accumulated layer landslide under the coupling action of earthquake and rainfall. *KSCE J Civ Eng* 27(1):98–108. <https://doi.org/10.1007/s12205-022-0110-9>
- Yao W, Zeng Z, Lian C, Tang H (2015) Training enhanced reservoir computing predictor for landslide displacement. *Eng Geol* 188:101–109. <https://doi.org/10.1016/j.enggeo.2014.11.008>
- Yanbin M, Hongrui L, Lin W, Wengang Z, Zhengwei Z, Haiqing Y, Luqi W, Xingzhong Y (2022) Machine learning algorithms and techniques for landslide susceptibility investigation: A literature review. *Tumu yu Huanjing Gongcheng Xuebao/J Civil Environ Eng* 44(1):53–67. <https://doi.org/10.11835/j.issn.2096-6717.2021.102>

- Yamaguchi Y, Makinoshima F, Oishi Y (2023) Simulating the entire rainfall-induced landslide process using the material point method for unsaturated soil with implicit and explicit formulations. *Landslides* 1–22. <https://doi.org/10.1007/s10346-023-02052-4>
- Yerro A, Girardi V, Martinelli M, Ceccato F (2022) Modelling unsaturated soils with the Material Point Method. A discussion of the state-of-the-art. *Geomech Energy Environment* 32:100343. <https://doi.org/10.1016/j.gete.2022.100343>
- Yin XC, Chen XZ, Song ZP, Yin C (1995) A new approach to earthquake prediction: The Load/Unload Response Ratio (LURR) theory. *Pure Appl Geophys* 145(3–4):701–715. <https://doi.org/10.1007/BF00879596>
- Yu X, Xia Y, Zhou J, Jiang W (2023) Landslide susceptibility mapping based on multitemporal remote sensing image change detection and multiexponential band math. *Sustainability (switzerland)* 15(3):2226. <https://doi.org/10.3390/su15032226>
- Yusof MKTM, Rashid ASA, Apandi NM, Khanan MFBA, Rahman MZBA (2023) A review of the application of support vector machines in landslide susceptibility mapping. *Disaster Advances* 16(11):71–83. <https://doi.org/10.25303/1611da071083>
- Zangmene FL, Ngapna MN, Ateba MCB, Mboudou GMM, Defo PLW, Kouo RT, Dongmo AK, Owona S (2023) Landslide susceptibility zonation using the analytical hierarchy process (AHP) in the Bafoussam-Dschang region (West Cameroon). *Adv Space Res* 71(12):5282–5301. <https://doi.org/10.1016/j.asr.2023.02.014>
- Zhang R, Gomaa SM, Hussein M, Zayed T, Meguid M (2023) Review of Numerical Approaches used in Soil-Pipe Interaction Analysis of Water Mains. *Transp Geotechnics* 101008. <https://doi.org/10.1016/j.trgeo.2023.101008>
- Zhang LL, Zhang J, Zhang LM, Tang WH (2011) Stability analysis of rainfall-induced slope failure: a review. *Proc Inst Civil Eng-Geotech Eng* 164(5):299–316. <https://doi.org/10.1680/jeng.2011.164.5.299>
- Zhang WJ, Chen YM, Zhan LT (2006) Loading/Unloading response ratio theory applied in predicting deep-seated landslides triggering. *Eng Geol* 82(4):234–240. <https://doi.org/10.1016/j.enggeo.2005.11.005>
- Zhao B, Dai Q, Han D, Dai H, Mao J, Zhuo L (2019) Probabilistic thresholds for landslides warning by integrating soil moisture conditions with rainfall thresholds. *J Hydrol* 574:276–287. <https://doi.org/10.1016/j.jhydrol.2019.04.062>
- Zhao B, Dai Q, Han D, Zhang J, Zhuo L, Berti M (2020) Application of hydrological model simulations in landslide predictions. *Landslides* 17(4):877–891. <https://doi.org/10.1007/s10346-019-01296-3>
- Zhu L, Huang JF (2006) GIS-based logistic regression method for landslide susceptibility mapping in regional scale. *J Zhejiang Univ-Sci A* 7(12):2007–2017. <https://doi.org/10.1631/jzus.2006.A2007>
- Zhu Y, Ishikawa T, Zhang Y, Nguyen BT, Subramanian SS (2022) A FEM-MPM hybrid coupled framework based on local shear strength method for simulating rainfall/runoff-induced landslide runout. *Landslides* 19(8):2021–2032. <https://doi.org/10.1007/s10346-022-01849-z>
- Zou Y, Zheng C (2022) A Scientometric analysis of predicting methods for identifying the environmental risks caused by landslides. *Appl Sci (switzerland)* 12(9):4333. <https://doi.org/10.3390/app12094333>